Multi-tissue proteomics identifies a link between satellite DNA organization and heritable transposon repression in *Drosophila*

Ankita Chavan[1,2,3¶], Lena Skrutl[1,2¶], Federico Uliana[1,3,#], Melanie Pfister[1], Franziska Brändle[1,2], Laszlo Tirian[4], Delora Baptista[5], Dominik Handler[4], David Burke[6], Anna Sintsova[7], Pedro Beltrao[8], Julius Brennecke[4], Madhav Jagannathan[1,3]*

[1]Institute of Biochemistry, ETH Zürich, Zürich, Switzerland

[2]Life Sciences Zürich Graduate School, Zürich, Switzerland

[3]Bringing Materials to Life Consortium, Zürich, Switzerland

[4]Institute of Molecular Biotechnology of the Austrian Academy of Sciences, Vienna BioCenter, Vienna, Austria

[5]Instituto Gulbenkian de Ciência, Oeiras, Portugal

[6]European Molecular Biology Laboratory, European Bioinformatics Institute (EMBL-EBI), Cambridge, UK

[7]Institute of Microbiology, ETH Zürich, Zürich, Switzerland

[8]Institute of Molecular Systems Biology, ETH Zürich, Zürich, Switzerland

[#]Present address – Johannes Gutenberg University Mainz, Mainz, Germany

*Corresponding author

E-mail: madhav.jagannathan@bc.biol.ethz.ch

[¶]These authors contributed equally to this work.

ABSTRACT

Non-coding satellite DNA repeats are abundant at the pericentromeric heterochromatin of eukaryotic chromosomes. During interphase, sequence-specific DNA-binding proteins cluster these repeats from multiple chromosomes into nuclear foci known as chromocenters. Despite the pivotal role of chromocenters in cellular processes like genome encapsulation and gene repression, the associated proteins remain incompletely characterized. Here, we use two satellite DNA-binding proteins, D1 and Prod, as baits to characterize the chromocenter-associated proteome in *Drosophila* embryos, ovaries, and testes through quantitative mass spectrometry. We identify D1- and Prod-associated proteins, including known heterochromatin proteins as well as proteins previously unlinked to satellite DNA or chromocenters, thereby laying the foundation for a comprehensive understanding of cellular functions enabled by satellite DNA repeats and their associated proteins. Interestingly, we find that multiple components of the transposon-silencing piRNA pathway are associated with D1 and Prod in embryos. Using genetics, transcriptomics, and small RNA profiling, we show that flies lacking D1 during embryogenesis exhibit transposon expression and gonadal atrophy as adults. We further demonstrate that this gonadal atrophy can be rescued by mutating the checkpoint kinase, *Chk2*, which mediates germ cell arrest in response to transposon mobilization. Thus, we reveal that a satellite DNA-binding protein functions during embryogenesis to silence transposons, in a manner that is heritable across later stages of development.

INTRODUCTION

'Heterochromatin' is classically defined as regions on eukaryotic chromosomes that remain condensed throughout the cell cycle[1]. The sequences that constitute heterochromatin mainly consist of simple non-coding tandem repeats known as satellite DNA [2] and interspersed repeats known as transposable elements (TEs) [3]. Both types of repeats can account for significant fractions of eukaryotic genomes and previous studies have suggested that they may propagate selfishly at the expense of overall organismal fitness. In addition, unrestricted expression of satellite DNA repeats and TEs can lead to adverse outcomes such as genome instability, chromosome mis-segregation and cell death[4–7]. However, accumulating evidence suggests important functions for regions enriched in these repetitive sequences. For example, satellite DNA repeats at the centromere have been proposed to function in the stable propagation of centromere identity[8,9] while pericentromeric satellite DNA repeats are thought to be important for chromosome pairing[10,11] and chromosome segregation[12,13]. Similarly, regulated activity of TEs can benefit cellular function[14] through roles in telomere maintenance[15], repeat copy number stability[16,17], genome restructuring[18] and the birth of new genes.

Within the nucleus, constitutive heterochromatin is organized into distinct domains that are separate from the more transcriptionally active euchromatin. For example, pericentromeric satellite DNA repeats from multiple chromosomes are clustered by satellite DNA-binding proteins into DNA-dense nuclear foci known as chromocenters, which typically remain transcriptionally silent[19,20]. This transcriptional silencing is orchestrated, in part, by the deposition of repressive post-translational modifications (PTMs) at target chromatin loci[19]. Once established, this repressive chromatin state can be heritably propagated, both across cell divisions within an organism as well as across generations [21–24]. Intriguingly, abrogation of heterochromatin-associated PTMs does not always perturb the highly condensed state and transcriptional inactivity of the underlying repetitive sequences[24,25].

In these instances, sequence-specific satellite DNA-binding proteins have been proposed as a complementary mechanism that maintains DNA compaction and transcriptional silencing at constitutive heterochromatin[24,25]. However, experimental evidence as to whether satellite DNA-binding proteins regulate transcriptional silencing at constitutive heterochromatin is lacking.

In *Drosophila*, we have shown that two sequence-specific DNA-binding proteins, D1 and Prod, contribute to chromocenter formation by clustering their cognate satellite DNA repeats [20,26,27]. Strikingly, chromocenter disruption through mutation of *D1* or *prod* leads to defective genome encapsulation in the form of micronuclei, which is associated with DNA damage and cell death[26,27]. However, these phenotypes occur in distinct tissues, with male germ cells acutely sensitive to *D1* mutation while larval imaginal discs fail to develop in the absence of Prod [26,27]. These findings point to potential tissue-specific differences in chromocenter composition and regulation. However, the chromocenter-associated proteome in distinct tissues remains largely unidentified since most proteomic studies have typically used constitutive heterochromatin proteins[28–30] or centromeric proteins[29,31,32] as baits in cultured cells.

In this study, we set out to identify chromocenter-associated proteins in multiple *Drosophila* tissues using quantitative mass spectrometry. We used the satellite DNA-binding proteins, D1 and Prod, as baits and identified chromocenter-associated proteins from embryos, adult ovaries and germline stem cell (GSC)-enriched adult testes. We have identified 495 proteins significantly enriched after affinity purification of D1 and Prod across all tissues. Interestingly, pathway analysis indicated that the D1- and Prod-associated proteome in embryos was enriched in DNA repair and transposon repression proteins. Following up on these data, we have identified an unanticipated molecular relationship between satellite DNA organization and TE repression in *Drosophila*. Taken together, our study lays the

102 groundwork toward a comprehensive understanding of the multi-faceted contributions of

103 satellite DNA repeats and their binding proteins to cellular function.

104 **RESULTS**

105 **Establishment and validation of strains carrying GFP-tagged satellite DNA-binding**

106 **proteins**

107 We performed affinity purification coupled to mass spectrometry (AP-MS) to identify
108 chromocenter-associated proteins in *Drosophila* embryos, ovaries and GSC-enriched
109 testes using D1 and Prod as baits (Fig. 1A). In nuclei from these tissues, D1 and Prod foci
110 were often found in proximity to each other (Fig. 1B), and we expected to identify common
111 interactors between the two baits. To minimize variability between baits, we used an affinity
112 purification strategy involving pulldown of GFP-tagged baits using GFP nanobody-coupled
113 beads. For D1, we made use of an available strain where GFP has been inserted upstream
114 of the endogenous locus. To validate this strain, we assessed the number of chromocenters
115 (D1 and Prod foci per cell) in male and female GSCs as well as fertility in both sexes in
116 comparison to a wild type reference strain (*D. melanogaster yw*). We observed that the
117 number of D1 and Prod foci per cell in male and female GSCs was identical to the wild type
118 (Fig. 1C, D), indicating that chromocenter formation was unperturbed in the GFP-D1 strain
119 in these cell types. In addition, we observed that homozygous GFP-D1 males and females
120 were fertile, although the fertility of homozygous GFP-D1 females is reduced compared to
121 the wild type (Fig. 1E, F). For Prod, we first generated a transgenic strain where a GFP-
122 tagged codon-optimized *Prod* was placed downstream of a 400 bp promoter sequence and
123 inserted into the attP40 locus (Fig. S1A). The *GFP-prod* transgene fully rescued the larval
124 lethality associated with loss-of-function *prod* mutations, $prod^{k01180}$ and $prod^{U}$ [33](Fig. S1B).
125 Hereafter, GFP-Prod refers to the *GFP-prod* transgene in a *prod* mutant background (*p400-*
126 *GFP-prod*, $prod^{k01180}/prod^{U}$) (Fig. S1B). We observed that the number of GFP-Prod foci was
127 at wild type levels in male and female GSCs (Fig. 1C, D), suggesting that the transgene
128 does not interfere with chromocenter formation in these cells. Like the GFP-D1 strain, GFP-
129 Prod males were fully fertile, while GFP-Prod females were sub-fertile in comparison to the

130 wild type (Fig. 1E, F). However, ovaries from both the GFP-D1 and GFP-Prod strains were
131 morphologically similar to the control (Fig. S1C), suggesting that early stages of oogenesis
132 are likely unaffected in these strains. As a negative control for GFP-D1 and GFP-Prod, we
133 used a strain ubiquitously expressing nucleoplasmic GFP (NLS-GFP). The NLS-GFP did not
134 enrich at chromocenters, and we observed that the number of chromocenters was
135 comparable to the wild type, GFP-D1 and GFP-Prod strains (Fig. 1C, D). Therefore, the
136 GFP-tagged D1 and Prod strains and the NLS-GFP control strain were used to characterize
137 the chromocenter-associated proteome in intact *Drosophila* tissues.
138
139 **Multi-tissue characterization of the chromocenter-associated proteome**
140 First, we optimized lysis and affinity purification conditions such that our bait proteins were
141 effectively solubilized (Fig. S1D) and immunoprecipitated (Fig. S1E). Following this, we
142 affinity purified GFP-D1, GFP-Prod (and NLS-GFP as a control) from the embryo, ovary and
143 testis lysates and identified the associated proteins by quantitative mass spectrometry.
144 While we were unable to analyze Prod pulldowns specifically in GSC-enriched testes due to
145 poor sample quality, we identified 495 proteins that were significantly enriched in the D1
146 and Prod pulldowns in comparison to the control pulldown of NLS-GFP across all tissues
147 ($\log_2$FC>1 and $p<0.05$, Fig. 2A-C, Fig. S2A, Table S1-3), with these hits likely representing
148 both direct and indirect interactions. In embryos, we identified that D1 co-purified known
149 chromocenter-associated or pericentromeric heterochromatin-associated proteins, such as
150 Su(var)3-9[34], ADD1[28,29], HP5[28,29], mei-S332[35], Mes-4[28], Hmr[29,36,37],
151 Lhr[29,36], and members of the chromosome passenger complex, such as borr and
152 Incenp[38] (Fig. 2A, Table S1). Prod pulldown in embryos co-purified chromocenter-
153 associated proteins such as Hcs[39] and Saf-B[40] (Table S1). Our proteomic data also
154 identified previously reported D1/Prod associations such as D1-ball (embryo), D1-RfC38
155 (ovary), D1-Smn (ovary), D1-Parp (embryo), Prod-CG15107 (ovary) and Prod-bocks
156 (embryo)[41,42]. Moreover, analysis of our proteomic data with STRING-DB[43] revealed

157 relationships between D1 and Prod co-purified proteins. For example, Prod co-purified
158 components of the replication protein A (RPA complex) (Fig. S2B), while D1 co-purified
159 multiple members of the origin recognition complex (ORC) (Fig. S2C) and the condensin I
160 complex (Fig. S2D).
161
162 We also observed a substantial overlap between D1- and Prod-associated proteins (yellow
163 points in Fig. 2A, B, Table S1-3), with 61 hits pulled down by both baits (blue arrowheads,
164 Fig. 2C) in embryos and ovaries. This observation is consistent with the fact that both D1
165 and Prod occupy sub-domains within the larger constitutive heterochromatin domain in
166 nuclei. Surprisingly, only 12 proteins were co-purified by the same bait (D1 or Prod) across
167 different tissues (magenta arrowheads, Fig. 2C, Table S1-3). In addition, only a few proteins
168 such as an uncharacterized DnaJ-like chaperone, CG5504, were associated with both D1
169 and Prod in embryos and ovaries (Fig. 2D). One interpretation of these results is that the
170 protein composition of chromocenters may be tailored to cell- and tissue-specific functions
171 in *Drosophila*. However, we also note that the large number of unidentified peptides in AP-
172 MS experiments means that more targeted experiments are required to validate whether
173 certain proteins are indeed tissue-specific interactors of D1 and Prod.
174
175 Finally, we used AlphaFold Multimer (AFM) to predict interaction interfaces for a subset D1
176 and Prod interactors ($\log_2$FC>2, $p<0.01$) from all tissues and potentially distinguish direct
177 versus indirect interactions[44]. AFM-based structural modeling has significantly advanced
178 identification of protein interaction interfaces and has been used across a wide variety of
179 organisms and protein types[45]. Moreover, the AFM-derived interface predicted template
180 modelling (ipTM) score has been used as a standard metric to evaluate the accuracy of the
181 structural models. Based on previous studies[44,46,47], ipTM scores above 0.5 represent a
182 medium confidence model of the interaction interface while ipTM scores above 0.8
183 represent high confidence models. Despite both D1 and Prod containing large intrinsically

184 disordered regions (IDRs), which hinder the accuracy of structural predictions, we found
185 that 6/78 D1 interactors and 16/79 Prod interactors yielded an ipTM score above 0.5 (Table
186 S4). Taken together, we have identified several proteins associated with the satellite DNA-
187 binding proteins, D1 and Prod across *Drosophila* tissues and AFM-based structural
188 modelling suggests that some of these hits could be direct interactors of D1 and Prod.
189
190 **DNA repair and TE repression proteins are co-purified by D1 and Prod in embryos**
191 Manual inspection of our data revealed that D1 and Prod pulled down multiple proteins
192 involved in DNA repair, such as Fancd2 (D1 and Prod), Top2 (D1 only), chrac-16 (D1 and
193 Prod) and the RPA complex (Prod only) in embryos (Fig. 2A, Table S5). Tandem repeats like
194 satellite DNA are inherently vulnerable to copy number changes[48] and are known to
195 employ specialized mechanisms during DNA repair[49–53]. Therefore, these interactions
196 may contribute to repeat homeostasis, especially during the rapid early embryonic
197 divisions. In addition, we identified that TE repression proteins (Table S6), such as the
198 canonical piRNA pathway members, Piwi (P-element induced wimpy testes) (Prod only) and
199 Maelstrom (Mael) (D1 and Prod) were also co-purified in embryos (Fig. 2A, Table S1).
200 Consistently, a hypergeometric test for pathway enrichment revealed that DNA repair and
201 TE repression proteins were enriched in the pulldowns from embryos and to a lesser extent
202 in other tissues (Fig. 2E).
203
204 **TE repression proteins are associated with chromocenters**
205 Transposable elements (TEs) are typically viewed as agents of genomic instability and their
206 unchecked mobilization is usually associated with DNA damage, mutation, cell death and
207 sterility[54]. In germline tissues from flies, as well as other metazoans, genome defense
208 against transposons requires a dedicated small RNA pathway known as the Piwi-interacting
209 RNA (piRNA) pathway[55,56]. In *Drosophila*, transcription of piRNA precursors is mediated
210 by a protein complex comprised of Rhino, Cutoff and Deadlock (RDC complex) [57–59],

211 followed by Nxf3-dependent nuclear export of precursor transcripts and processing into
212 mature piRNAs[55,56]. Mature piRNAs are loaded onto a family of RNA-binding Argonaute
213 proteins including Piwi (P-element induced wimpy testis), a canonical member of the piRNA
214 pathway [55,56]. piRNA-bound Piwi enters the nucleus, locates genomic TE loci through
215 sequence complementarity and mediates TE repression through local heterochromatin
216 formation and chromatin compaction. Heterochromatin-associated proteins such as Hybrid
217 male rescue (Hmr)[36], Lethal hybrid rescue (Lhr)[36] and small ovary (Sov)[60–62] are
218 implicated in heterochromatin formation and transcriptional repression at transposon
219 loci[60]. All three proteins were co-purified by D1 in embryos in this study. In addition,
220 recent studies in cultured cells of embryonic origin have also identified that both Piwi and
221 Hmr interact with Prod [63]. These data support the notion that satellite DNA-binding
222 proteins may contribute to piRNA pathway function, potentially through regulating
223 heterochromatin stability at TE loci.
224
225 In order to validate our proteomics data, we used strains where either Piwi, which is a
226 canonical piRNA pathway Argonaute protein, or Sov, which is implicated in piRNA-
227 dependent heterochromatin formation at TEs[60–62], were tagged with GFP. Although Piwi
228 mediates transcriptional repression at TE loci, it is localized throughout the entire nucleus
229 and the GFP-Piwi signal expectedly overlapped with the heterochromatic D1 and Prod foci
230 in embryonic nuclei (Fig. 3A). In contrast, Sov, which is recruited to transposon loci by the
231 piRNA pathway protein Panoramix[60], exhibited a punctate GFP signal in embryonic
232 nuclei, which was frequently present at the boundaries of D1/Prod-containing
233 chromocenters (Fig. 3A). We observed a similar pattern for GFP-Piwi and Sov-GFP
234 localization in adult germ cells from males and females (Fig. S3A-D). Moreover, the D1-
235 interacting heterochromatin protein, Hmr, which contributes to TE repression[36], was also
236 observed at the chromocenter boundary (Fig. S3E, F), in agreement with recent reports
237 suggesting that Hmr may bridge centromeric and pericentromeric heterochromatin[29,32].

238

239 To further test the potential associations between D1/Prod and Piwi, we performed a
240 reciprocal AP-MS experiment using embryonic lysates from the GFP-Piwi strain (and the
241 NLS-GFP strain as a control) (Fig. 3B, Table S7). Piwi co-purified proteins identified as
242 D1/Prod interactors in embryonic lysates (red points, Fig. 3B). Strikingly, four proteins
243 (CG14715, Fit, CG10208 and Ugt35D1) were high confidence hits from the Piwi, D1 and
244 Prod pulldowns (Fig. 3C). All these proteins are relatively unstudied. CG14715 is an
245 uncharacterized FK506-binding protein, while Ugt35D1 is a putative UDP-
246 glycosyltransferase. Female independent of transformer (Fit) is a sexually dimorphic small
247 peptide that has been implicated in feeding control[64], while CG10208 is an
248 uncharacterized protein with no known domains or function. To determine how these
249 proteins may potentially interact with each other and with D1, Prod and Piwi, we used AFM
250 to model interaction interfaces between all possible pairs (Table S8). Interestingly, 8/28 of
251 the protein pairs had ipTM scores above 0.5 (blue and red points, Fig. 3D), with these
252 medium and high confidence scores highlighting interfaces that may give rise to direct
253 interactions. Among these, both D1 and Prod had medium confidence interfaces with Piwi,
254 which were mediated by contacts between disordered regions on D1 and Prod that
255 threaded through a central cleft in the Piwi protein (Fig. S4A). At the same time, we were
256 unable to detect a Piwi-D1 interaction by co-immunoprecipitation from embryonic lysates
257 (Fig. S4B), suggesting that this interaction may only occur in a small subset of cells (e.g.
258 germ cells) in embryos or that the interaction may be mediated by weak/transient
259 associations between disordered regions. Overall, the data from the proteomic, microscopy
260 and structural modeling experiments strongly hint at a functional relationship between
261 satellite DNA organization and the piRNA pathway.

262

263 **Satellite DNA clustering into chromocenters does not rely on piRNA pathway proteins**

264 Repressive histone post-translational modifications, such as H3K9me2/3, are enriched at
265 pericentromeric heterochromatin[13,25] and recent studies identifying piRNAs
266 complementary to complex satellite DNA repeats [65] suggest that the piRNA pathway may
267 promote repressive PTMs at satellite DNA repeats and facilitate chromocenter formation.
268 This idea was supported by prior studies showing that an interaction between Piwi and the
269 heterochromatin protein, HP1, contributes to heterochromatin organization in both somatic
270 and germ cells [66–68]. Since Piwi mutation results in a severe agametic phenotype in
271 ovaries and testes, we instead used mutations of aubergine, which mediates piRNA
272 amplification through the ping-pong mechanism[56]. In the absence of aubergine, total
273 piRNA levels are decreased and piRNA-free Piwi fails to enter the nucleus[69]. We observed
274 that aubergine mutation (aub^{HN2}/aub^{QC42}) as well as germline knockdown of aubergine
275 resulted in a mild de-clustering of Prod foci in female GSCs but had no effect on the
276 number of D1 foci in the same cells (Fig. S5A-C). These findings suggest that the piRNA
277 pathway does not have a prominent role in chromocenter stability in female GSCs.
278
279 **Satellite DNA-binding proteins make a subtle contribution to TE repression in adult**
280 **ovaries**
281 For an initial assessment of whether D1 and Prod contribute to TE repression, we used
282 established reporters of transposon activity in the adult germline (*GFP-Burdock-lacZ*) and
283 adult soma (*gypsy-lacZ*) of *Drosophila* ovaries [70,71]. In the gonadal soma, we used the *tj-*
284 *gal4* driver to express RNAi against D1 in a genetic background containing the *gypsy-lacZ*
285 reporter. Despite effective depletion of D1 (Fig. S6A), we did not observe increased
286 expression of the TE reporter (*gypsy-lacZ*) based on staining for beta-galactosidase (β-Gal)
287 in comparison to the negative control (mCherry RNAi) (Fig. S7A). Similar to D1 depletion,
288 Prod depletion did not result in de-repression of *gypsy-lacZ* in the somatic follicle cells (Fig.
289 S6B, Fig. S7A). In contrast, RNAi-mediated depletion of Sov, which is required for TE

290 repression in gonadal somatic cells[61,62], resulted in β-Gal signal in the follicle cells across
291 multiple stages of oogenesis, indicating expression of the somatic TE reporter (Fig. S7A).
292 Next, we tested whether loss of D1 in the germline resulted in increased expression of the
293 germline TE reporter, *GFP-Burdock-lacZ*. To do so, we used a previously validated mutant
294 allele ($D1^{LL03310}$) in trans to a chromosomal deficiency spanning the D1 locus ($Df(3R)^{Bsc666}$) in
295 a background containing *GFP-Burdock-lacZ*[26]. Here, we did not observe GFP signal in
296 the germline cells of both *D1* mutant ovaries and the heterozygous controls (Fig. S7B).
297 Similarly, RNAi-mediated Prod depletion (Fig. S6C) in a background containing *GFP-*
298 *Burdock-lacZ* also did not lead to observable GFP signal in the ovaries (Fig. S7B). In
299 contrast, depletion of aubergine, which is required for TE repression in germ cells, resulted
300 in a strong germline GFP signal (Fig. S7B). These data suggest that D1 and Prod do not
301 contribute to the repression of *gypsy* and *Burdock* during oogenesis. In addition, previous
302 studies have determined that Prod depletion in adult ovaries does not alter the expression
303 of other TEs such as *HeT-A*, *TAHRE* and *blood* [70,71]. However, we cannot exclude from
304 these data that D1 and Prod contribute to the repression of other TEs.
305
306 Therefore, we performed RNA sequencing to determine transcriptome-wide effects on TE
307 expression. Since Chk2 arrests germ cell development in response to TE de-repression and
308 DNA damage[72,73], we used heterozygous and *D1* mutant ovaries in a *chk2* mutant
309 ($chk2^{6006}$) background to prevent developmental arrest of potential TE-expressing germ
310 cells. We observed that both genotypes exhibited similar gonad morphology (Fig. 4A).
311 Consistent with our data from the TE reporters and previous studies, expression of most TE
312 families was not elevated in *D1* mutant ovaries in comparison to the heterozygous control
313 (Fig. 4B, Table S9). One exception was the LTR retrotransposon *tirant,* which was
314 expressed 5-6-fold higher in *D1* mutant ovaries. However, the magnitude of TE expression
315 in the *D1* mutant ovaries is not in the range of what has been observed for ovaries that lack

316 canonical piRNA pathway proteins[59,74]. The mild increase in *tirant* expression is therefore
317 unlikely due to compromised piRNA pathway function.
318
319 **Levels of TE-targeting piRNAs are largely unperturbed in the absence of D1**
320 Since transposon silencing by the piRNA pathway relies on the production of piRNAs and
321 their loading onto the Piwi, Aub and Ago3 Argonaute proteins[56], we performed small RNA
322 sequencing to determine whether the Argonaute-bound piRNA pool was altered in *D1*
323 mutant ovaries in comparison to heterozygous control ovaries. Our data show that total
324 levels of mature piRNAs, normalized to miRNA reads, are not substantially affected by the
325 loss of D1 (Fig. 4C, D). We also did not observe a marked reduction in antisense piRNAs
326 complementary to TEs in *D1* mutant ovaries, including those mapping to *tirant* (Fig. 4E). Our
327 data indicate that the biogenesis of TE-mapping piRNAs is unaffected in the absence of D1.
328 Furthermore, our RNA-seq data also demonstrated that none of the 347 genes that are
329 known to contribute to TE silencing (Table S6) were differentially expressed in *D1* mutant
330 ovaries (blue points, Fig. 4F, Table S9). Altogether, our data suggest that the subtle
331 changes in the expression of a few TEs in *D1* mutant ovaries are unlikely due to
332 compromised piRNA biogenesis or altered expression of piRNA pathway components.
333 Rather, we propose that impaired heterochromatin stability in the *D1* mutant is the
334 underlying cause.
335
336 **The piRNA biogenesis machinery is mislocalized to satellite DNA in the absence of D1**
337 In contrast to TE transcripts, we observed that transcripts corresponding to the abundant
338 1.688g/cm^3 satellite DNA repeat (denoted as *SAR DM* and *SAR2 DM*, Fig. 4B) were
339 upregulated in *D1* mutant ovaries in comparison to the heterozygous control. Conversely,
340 transcripts mapping to the Responder (Rsp) satellite DNA repeat were downregulated in the
341 absence of D1 (Fig. 4B). These changes in satellite DNA transcription were correlated with
342 changes in piRNAs originating from these repetitive loci (Fig. 4E). We further mapped the

343 small RNA reads to the different monomers that make up the 1.688 g/cm^3 satellite DNA and
344 found a specific upregulation of the 260bp and 359bp variants (Fig. 4E).
345
346 Recent studies have demonstrated that the Rhino-Deadlock-Cutoff complex stimulates
347 transcription of complex satellite DNA repeats, which are then processed into mature
348 piRNAs [65,75]. Interestingly, the absence of a ZAD-zinc finger DNA-binding protein known
349 as Kipferl causes the RDC complex to mislocalize to and transcribe the 359 and Rsp
350 satellite DNA repeats at higher levels in ovaries[75]. Based on our observation that *D1*
351 mutant ovaries exhibit upregulated transcripts and piRNAs corresponding to the 359bp
352 satellite DNA (Fig. 4B, E), we tested whether D1 may also regulate the localization of the
353 RDC complex during oogenesis. To do so, we used a strain expressing GFP-tagged Cutoff
354 (EGFP-Cuff) to assess RDC complex localization in ovarian nurse cells, where
355 pericentromeric satellite DNA repeats from all chromosomes are clustered into a single
356 prominent DAPI-dense and D1-enriched chromocenter (arrowhead, Fig. 5A). In the EGFP-
357 Cuff strain, we observed that Cuff was localized to the periphery of the nurse cell
358 chromocenter and was also present at many sites across the nucleus, consistent with the
359 presence of piRNA clusters at pericentromeric heterochromatin and chromosome arms
360 (Fig. 5A, Fig. S8A-B). We next examined Cuff localization in *D1* mutant nurse cells in
361 comparison to the heterozygous control. In both the heterozygous control and *D1* mutant,
362 DAPI-dense chromocenters were still detected in nurse cells (yellow arrowheads, Fig. 5B).
363 However, we observed an approximately 3-fold increase in chromocenter size in nurse cells
364 lacking D1 (Fig. 5B-C), likely due to impaired satellite DNA clustering. Strikingly, this
365 increase in chromocenter size in *D1* mutants was accompanied by a substantial mis-
366 localization of Cuff to satellite DNA (Fig. 5B, D), where we observed ~6-fold more Cuff at *D1*
367 mutant chromocenters in comparison to the heterozygous control (Fig. 5B, D). In addition,
368 we observed that the expanded chromocenters in the *D1* mutant nurse cells were also
369 positive for Nxf3 (Fig. 5E), which normally colocalizes with Cuff at piRNA clusters and

370 mediates nuclear export of piRNA precursors[76,77]. Consistently, RNA *in situ* hybridization
371 revealed increased transcription of the 359 satellite DNA repeat at the expanded Cuff-
372 positive chromocenters in *D1* mutant nurse cells (Fig. 5F, G). Finally, the 359bp probe signal
373 was abolished following RNase A treatment (Fig. 5H), which is further indication that the
374 359bp satellite DNA repeat is aberrantly transcribed following loss of D1. Our data indicate
375 that D1 inhibits RDC localization to certain complex satellite DNA repeats in *Drosophila*
376 ovaries. However, unlike in *Kipferl* mutant ovaries, the RDC mislocalization in *D1* mutant
377 ovaries did not have a substantial effect on the levels of piRNAs targeting TEs and TE
378 silencing. Altogether, the TE reporter experiments, gene expression analysis and small RNA
379 sequencing suggest that TE repression in the germ cells and somatic cells of adult gonads
380 is largely independent of D1 or Prod.
381
382 **Maternal and zygotic D1 contribute to TE repression in adult gonads**
383 Although D1 and Prod appear to be dispensable for TE repression in adult gonads, our
384 proteomic data identified that TE repression proteins were mainly co-purified by D1 and
385 Prod in embryos. Thus, testing the functional relevance of these interactions required
386 depleting satellite DNA-binding proteins during embryogenesis. This experiment is
387 challenging since F_1 mutants (the progeny of heterozygous parents) contain maternal
388 deposits during embryogenesis (Fig. S9A-C) and protein/RNA depletion experiments can be
389 ineffective in early embryos[78]. However, the progeny of F_1 mutants (F_2 mutants) lack both
390 maternal and zygotic protein (Fig. S9A-C) and allow us to test the role of satellite DNA-
391 binding proteins in TE repression during embryogenesis. Since *D1* mutants are viable and
392 fertile (unlike *prod* mutants, which are larval lethal[33]), we chose to assess TE repression in
393 F_1 *D1* mutants, F_2 *D1* mutants and their associated heterozygous controls (Fig. S9A-C).
394 Briefly, the F_1 *D1* mutant lacks zygotically expressed D1 but retains a maternal contribution
395 during embryogenesis and potentially early larval development (Fig. S9A, C). In comparison,
396 the F_1 *D1* heterozygote contains both maternally contributed and zygotically expressed D1

397 (Fig. S9A, C). In the F_2 *D1* mutants, which are the progeny of F_1 *D1* mutant females, both
398 maternal and zygotic D1 are absent during embryogenesis and adulthood (Fig. S9B, C),
399 while the corresponding F_2 *D1* heterozygote lacks maternal D1 in the early embryo but
400 expresses D1 upon zygotic genome activation (Fig. S9B, C).
401
402 We initially assessed female gonad morphology in the above genotypes since unrestricted
403 transposon expression can result in arrested germ cell development and agametic
404 ovaries[4,79]. Strikingly, we observed that F_2 *D1* mutant females predominantly exhibited
405 agametic ovaries (Fig. 6A), with the vast majority of ovarioles either lacking any discernible
406 Vasa-positive germ cells or containing only undifferentiated Vasa-positive germ cells, which
407 did not develop into cysts (Fig. 6B, C). Moreover, the failure of germline development and
408 agametic ovaries in the F2 *D1* mutant strongly correlated with loss of female fertility (Fig.
409 6D). Interestingly, the presence of either maternal or zygotic D1 was sufficient to rescue this
410 phenotype, as gonad morphology and early germ cell development of both the F_1 *D1*
411 mutant females (maternal D1 only) and the F_2 *D1* heterozygote females (zygotic D1 only)
412 were mostly unaffected (Fig. 6A-C), even though both genotypes exhibited more variable
413 fertility (Fig. 6D). We next tested whether certain transposons were expressed in F_2 *D1*
414 mutant ovaries using single molecule RNA *in situ* hybridization (smFISH). Here, we
415 observed that the *copia* retrotransposon, but not other TEs such as *burdock* or *gypsy*, was
416 highly expressed in ~70% of early germ cells from F_2 *D1* mutant ovaries (Fig. 6E-G). In
417 comparison, *copia* expression was not elevated in early germ cells from the *yw* wild type
418 strain or in the F_1 *D1* mutant (Fig. 6A). While ~90% of the *aubergine* mutant germaria
419 (positive control) contained *copia* expressing germ cells (Fig. 6E, F), this expression was
420 mostly restricted to differentiated germ cell cysts; undifferentiated *aubergine* mutant germ
421 cells (GSCs and cystoblasts, arrowheads, Fig. 6E) exhibited a markedly lower level of *copia*
422 expression (Fig. 6G). Thus, the high level of transposon expression, occurring in the early
423 germ cells of F_2 *D1* mutants, may contribute to the loss of GSCs or block their

424 differentiation, ultimately leading to agametic gonads. Consistently, we found that *chk2*
425 mutation rescues the agametic gonads in the F_2 *D1* mutant (Fig. 6H, I). Together, our data
426 reveal embryogenesis (or potentially early larval development) as a critical period when the
427 presence of maternal and/or zygotic D1 is sufficient for establishing TE silencing, which can
428 then be heritably maintained throughout development (Fig. 7).

429 **Discussion**

430 In this study, we have characterized the chromocenter-associated proteome across
431 *Drosophila* embryos, ovaries and GSC-enriched testes using two known satellite DNA-
432 binding proteins, D1 and Prod, as baits. We have identified 495 potential interactions
433 across three different tissues encompassing known heterochromatin-associated proteins,
434 DNA repair enzymes, proteins involved in transposon repression and a host of
435 uncharacterized proteins. Interestingly, we found a tissue-specific signature for the
436 chromocenter proteome, with D1 and Prod associating with many common proteins per
437 tissue and relatively few common proteins per bait across the tissues. This finding suggests
438 that the tissue-context or cellular function may be a primary determinant of the
439 chromocenter proteome. In addition, our structural predictions using AFM highlight
440 potential interfaces that may mediate direct interactions between D1, Prod and their
441 associated proteins. We suggest that these high-scoring hits represent promising avenues
442 of research that will expand our knowledge of satellite DNA biology and chromocenter
443 function.

444

445 Since islands of TE are often embedded within vast tracts of satellite DNA[3,17,80], we
446 were intrigued by the hits from the piRNA pathway, which were predominantly identified in
447 embryos. Here, we observed that the absence of D1 during embryogenesis (the F_2 *D1*
448 mutant) led to a striking elevation of TE expression and Chk2-dependent tissue atrophy in
449 adult ovaries. Similarly deleterious phenotypes were not observed in adult ovaries, when
450 either only maternally deposited D1 (the F_1 *D1* mutant) or only zygotically expressed D1 (the
451 F_2 *D1* heterozygote) were present during embryogenesis. These data suggest that the
452 presence of D1 throughout development is not *per se* required for TE repression. Rather,
453 our findings point to embryogenesis as the likely window of time during which D1
454 contributes to heritable TE silencing in germ cells. They also explain why approaches such
455 as RNAi-mediated knockdown or mutation in the F_1 generation, where D1 likely persists

456 during embryogenesis, do not result in TE expression. Our results also echo previous
457 observations that embryonic Piwi is important for heterochromatin-dependent gene
458 silencing in adults[68], although it should also be noted that the role of embryonic Piwi in
459 transposon silencing is more limited[81,82].
460
461 How could a satellite DNA-binding protein like D1 contribute to heritable silencing at TE
462 loci? While the D1-dependent clustering and compaction of satellite DNA repeats may
463 shield satellite DNA-embedded TE loci from transcription factors, this alone does not
464 explain how TEs remain silenced throughout development in the absence of D1 (e.g. the F_1
465 *D1* mutant). Rather, we propose that biophysical properties associated with the
466 condensation of satellite DNA repeats into chromocenters could play an important role. For
467 example, the intrinsically disordered regions (IDRs) present in D1 and Prod[83], could
468 facilitate the selective partitioning of client proteins into chromocenters. Potential client
469 proteins could include piRNA-dependent heterochromatin proteins such as Hmr, Lhr and
470 Sov, canonical piRNA pathway proteins such as Piwi and Mael or other D1/Prod-interacting
471 heterochromatin proteins identified in this study. In essence, satellite DNA-binding proteins
472 may foster an environment at satellite DNA-embedded TE loci during embryogenesis that
473 facilitates the deposition of repressive PTMs and ensures heritable transcriptional
474 repression.
475
476 In summary, our study has characterized the chromocenter-associated proteome across
477 three *Drosophila* tissues. We have revealed an unanticipated relationship between satellite
478 DNA organization and heritable transposon repression. The as-of-yet uncharacterized hits
479 identified in this study establish a path toward revealing the full scope of satellite DNA and
480 chromocenter function in *Drosophila* as well as other eukaryotes.
481
482

483 **Materials and Methods**

484 **Fly husbandry and strains.** All fly stocks were raised on standard Bloomington medium at
485 25°C unless otherwise indicated. *D. melanogaster y w* was used as a wild type stock. *prod*^{U}
486 (BDSC42686), *GFP-D1* (BDSC50850), *Ubi-NLS-GFP* (BDSC5826, BDSC5826), *Df(3R)*^{Bsc666}
487 (BDSC26518), *aub*^{QC42} (BDSC4968), *aub*^{HN2} (BDSC8517), *piwi*^{1} (BDSC43637), *piwi*^{2}
488 (BDSC43319), *UAS-Dcr-2* (BDSC24650), *mCherry* ^{RNAi} (BDSC35785) and *aub* ^{RNAi}
489 (BDSC39026) were obtained from the Bloomington *Drosophila* stock center. *D1*^{LL03310}
490 (DGRC140754) and *FRT42D prod*^{k08810} (DGRC111248) were obtained from the Kyoto stock
491 center. *GFP-Burdock-lacZ* (v313212), *tj-gal4, gypsy-lacZ* (v313222), *GFP-Piwi* (v313321),
492 *EGFP-Cuff* (v313269), *D1* ^{RNAi} (v101946) and *Prod* ^{RNAi} (v106593) were obtained from the
493 Vienna Drosophila Resource Center. *Hmr-HA*[36] was a gift from Daniel Barbash. Sov-GFP
494 (*sov*^{def1}; *Dp(1;2)*^{FF025056})[61] was a gift from Ferenc Jankovics. *nos-gal4* (second
495 chromosome insertion) and *chk2*^{6006} were gifts from Yukiko Yamashita. *nos-gal4* (third
496 chromosome insertion)[84] and UAS-Upd[85] have been previously described.

497 **Construction of the GFP-Prod strain.** First, a 400bp promoter upstream of the Prod start
498 site from *D. melanogaster* was PCR amplified using the following primer pair,
499 GATCAAGCTTCTGTTGTTATGCATATCGTTC and
500 GATCGAATTCCCGGGTATCCTTGCTC and subcloned into the HindIII and EcoRI sites on
501 *pUASt-GFP-attB*, replacing the UAS sequence. Subsequently, a codon-optimized Prod
502 sequence was inserted downstream of the GFP, and transgenic flies were generated using
503 PhiC31 integrase-mediated transgenesis into the *attP40* site (BestGene). The GFP-Prod
504 allele was generated by recombining the *p400-GFP-Prod* transgene with *prod*^{k08810}. Two
505 virgin *prod*^{U} females were crossed to single tester male carrying either the *p400-GFP-Prod*,
506 *prod*^{k08810} allele or the *prod*^{k08810} allele as a control in vials at 25°C. The percent of trans-
507 heterozygous *prod* mutant flies was quantified in each replicate.

508 **Fertility assay.** For male fertility assays, a single tester male was maintained with two virgin
509 *y w* females in vials for 7d and the number of resulting progenies was counted until 20 days
510 post setup. For female fertility assays, a single tester female was maintained with two *y w*
511 males in vials for 7d and the number of resulting progenies was counted until 20 days post
512 setup. Vials that contained any deceased parent flies were omitted from the analysis.

513 **Immunofluorescence staining.** Immunofluorescence staining of *Drosophila* tissues was
514 performed as follows. For fixation, adult tissues were dissected in PBS, transferred to 4%
515 formaldehyde in PBS and fixed for 30 minutes. Fixation of *Drosophila* embryos was
516 performed using a standard protocol. Briefly, collected embryos were moved to glass
517 scintillation vials and washed three times with 1x PBS, dechorionated using 3 ml of 50%
518 bleach solution for 90 secs by vigorous shaking and washed again in 1x PBS five times to
519 remove the bleach. Dechorionated embryos were fixed using a heptane: 4%
520 paraformaldehyde (PFA) (1:1) solution by vigorously shaking for 20 minutes. Following
521 fixation, the bottom aqueous phase was removed and ice cold methanol was added to
522 devitellinize the fixed embryos. After this step, embryos were washed three times in ice-cold
523 methanol and stored in methanol at -20°C for further use. Prior to immunofluorescence
524 staining, embryos were rehydrated using serial washes of methanol: PBS-T at 4:1, 1:1 and
525 1:4 volumes and followed by one wash in 1x PBS-T for 5 min each. For immunostaining,
526 fixed tissues were washed in 1x PBS-T (PBS containing 0.1% Triton-X) for at least 60
527 minutes, followed by incubation with primary antibody in 3% bovine serum albumin (BSA) in
528 PBS-T at 4°C overnight. Samples were washed three times in PBS-T, incubated with
529 secondary antibody in 3% BSA in PBS-T at 4°C overnight, washed as above, and mounted
530 in VECTASHIELD with DAPI (Vector Labs). Fluorescent images were taken using a Leica
531 TCS SP8 confocal microscope with 63x oil-immersion objectives (NA=1.4). Images were
532 processed using Adobe Photoshop or ImageJ.

533 **RNA in situ hybridization.** RNA *in situ* hybridization on ovaries was performed as
534 previously described[86]. Briefly, 3-4 ovaries were dissected in RNase-free 1x PBS and fixed
535 in 3.7% formaldehyde in PBS for 30 minutes on a nutator with gentle shaking. Following
536 fixation, samples were washed with RNase-free 1x PBS three times and subsequently
537 incubated in ice-cold ethanol at 4°C overnight on a nutator. The next day, samples were
538 washed with RNase-free wash buffer (2XSSC, 10% formamide) for 3 minutes at room
539 temperature and subsequently incubated with the hybridization mix (50-125 nM probes, 2x
540 SSC, 10% dextran sulfate, 1g/L *E.coli* tRNA, 2mM vanadyl ribonucleoside complex, 0.5%
541 Rnase-free BSA and 10% deionized formamide) at 37°C overnight. Samples were then
542 washed twice (wash buffer) at 37°C for 30 minutes each and mounted in VECTASHIELD
543 with DAPI (Vector Labs). The following probe was used to hybridize to the 359bp satellite
544 plus strand (AGGATTTAGGGAAATTAATTTTTGGATCAATTTTCGCATTTTTTGTAAG).
545 Stellaris RNA FISH probes against the full-length Burdock consensus sequence were
546 synthesized (LGC Biosearch technologies). Stellaris RNA FISH probes targeting Het-A and
547 Copia were gifts from Yukiko Yamashita. An oligo-dT probe was used to hybridize to
548 polyadenylated RNA. Fluorescent images were taken using a Leica TCS SP8 confocal
549 microscope with 63x oil-immersion objectives (NA=1.4). Images were processed using
550 Adobe Photoshop.

551 **Image Analysis.** All image analysis was performed using ImageJ. For the quantitation of
552 relative chromocenter size, we demarcated a region of interest (ROI^N) encompassing the
553 entire nucleus as well as second ROI encompassing only the chromocenter (ROI^C) for each
554 nurse cell (stages 4-6) analyzed. ROI^C/ROI^N equals the relative chromocenter size. For
555 enrichment of EGFP-Cuff at chromocenters, we estimated the total EGFP-Cuff signal in
556 ROI^C and divided it by the total EGFP-Cuff signal in ROI^N to give the percentage of EGFP-
557 Cuff at chromocenters. For the normalized estimation of Copia expression, we estimated
558 the average intensity of nuclear Copia (ROI^{Copia}) and normalized this value to the three

559 cytoplasmic ROIs that estimated the average intensity of total mRNA based on the oligo-dT
560 probe. For the normalized estimation of 359 transcripts at chromocenters, we estimated the
561 average intensity of 359 probe signal at chromocenters (ROI^C) for each nurse cell and
562 normalized this value to a cytoplasmic ROI that have background fluorescence.

563 **Isolation of nuclei from embryos.** Flies reared in population cages were allowed to lay
564 eggs on fresh yeast paste for ~18 hours. Embryos were collected using a set of sieves,
565 washed with 1X PBS and dechorionated using 50% bleach. Next, embryos were moved to a
566 dounce homogenizer containing light nuclear buffer (15 mM Tris-HCl pH 7.4, 60 mM KCl,
567 5 mM $MgCl_2$, 15 mM NaCl2 and 1 M sucrose) supplemented with 1x protease inhibitor
568 cocktail (PIC, Roche,11697498001)and 1mM PMSF. The homogenate was then incubated
569 on ice for 5 minutes and filtered through 2 layers of Miracloth tissue (Calbiochem). The
570 filtered homogenate was then centrifuged for 20 min at 480 rpm at 4°C to pellet any debris.
571 The supernatant containing nuclei was transferred into a fresh tube and the nuclei were
572 pelleted at 4000 g for 30 min at 4°C. The pellet was then resuspended in 1 ml light nuclear
573 buffer containing 0.1 mM EDTA and the nuclei were again centrifuged at 16000 g for 5
574 minutes before lysis.

575 **Tissue lysis.** Nuclei isolated from embryos were lysed for 90 min at 4°C with extraction
576 buffer (15 mM Tris-HCl pH 7.4, 60 mM KCl, 5 mM $MgCl_2$, 450 mM NaCl2, 1% Triton-X
577 [vol/vol], 500 units of benzonase) 1X PIC and 5 μl/ml PMSF). The resulting lysate was
578 separated from the insoluble chromatin by centrifugation for 20 min at 14000 g at 4°C. For
579 each ovary replicate, ~ 200 pairs were dissected from <1d old flies, flash frozen with liquid
580 nitrogen and stored at -80°C prior to lysis. 500µl of ice-cold lysis buffer (450 mM NaCl,
581 50mM Tris-HCl (pH-7.5), 5% glycerol, 1mM MgCl2, 1mM EDTA, 0.2% NP40, 0.5mM DTT,
582 1x PIC, 5 μl/ml PMSF) was added to frozen ovaries, which were then homogenized with a
583 motorized pestle until complete breakdown of the tissue. After homogenization, samples

584 were incubated with benzonase (Sigma Aldrich, 2 µl/500 µl of lysate) for 90 minutes at 4°C
585 on a rotating wheel. Following this, samples were first centrifuged for 3 min at 10000 g at
586 4°C to precipitate the debris from the tissues, homogenized again for 30 secs and
587 centrifuged for 5 min at ~18700 g at 4°C. The supernatant (without the surface lipid layer)
588 was transferred to a new 1.5 ml tube and centrifuged again for 5 min at ~18700g prior to
589 use. For each testis replicate, ~100 pairs of GSC-enriched (nos-gal4 > UAS-Upd) testis
590 tumors were dissected, flash frozen with liquid nitrogen and stored at -80°C prior to lysis.
591 300 µl RIPA lysis buffer [450 mM NaCl, 0.5 % NP-40 [vol/vol], 0.5 % Sodium deoxycholate
592 [mass/vol], 0.1 % SDS, 50 mM Tris pH 7.4] containing 1x protease inhibitor cocktail (PIC)
593 (Roche,11697498001) and 5 µl/ml PMSF (Sigma-Aldrich, P7626) was added to frozen
594 testes for 10 min. Tissue disruption was performed by applying 20 strokes with the tight
595 pestle in a 1 ml dounce homogenizer, the samples were incubated for another 20 minutes on
596 ice following which benzonase was added for 1 hour at 10°C. Homogenized lysates were
597 centrifuged at 14000 g for 20 min at 4°C prior to use. GFP-Piwi and NLS-GFP embryos were
598 collected as indicated in the previous section, dechorionated, flash frozen with liquid nitrogen
599 and stored at -80°C prior to lysis. Embryo lysis for these samples was performed in an
600 identical manner to the ovary lysis above.

601 **Affinity purification and mass spectrometry.** Affinity purification was performed using
602 anti-GFP nanobody coupled magnetic beads (~ 30µl slurry) (Chromotek AB_2631358).
603 Briefly, beads were collected using a magnetic rack, washed three times using the lysis
604 buffer and incubated with the lysate for 90 minutes on a rotating wheel at 4°C. After the
605 incubation, beads were washed three times for 5 minutes with a wash buffer (450 mM NaCl,
606 50mM Tris-HCl (pH-7.5), 1mM MgCl2, 1 mM EDTA, 0.5mM DTT) at room temperature.
607 Washed beads containing the protein complexes were subjected to on-beads proteolysis.
608 Samples were transferred into a 10kDa molecular weight cutoff spin column (Vivacon 500,
609 Sartorious), following the FASP protocol[87]. Beads in solution were dried, denaturated (8M

610 Urea), reduced (5mM TCEP, 30min 37C) and alkylated (10mM Iodoacetamide, 30min 37C).
611 Beads were then washed three times with 50mM ammonium bicarbonate (250µl). During
612 the buffer exchange, samples were centrifuged at 10000g. Subsequently, samples were
613 proteolyzed with 0.5µg of Trypsin (Promega, sequencing grade) for 16h at 37°C. The
614 proteolysis was quenched with 5% formic acid and peptides were subjected to C18
615 cleanup (BioPureSPN PROTO 300 C18, Nest group), following the manufacturer's
616 procedure. The eluted peptides were then dried using a speedvac and resuspended in 20µl
617 of 2% acetonitrile and 0.1% formic acid.

618 **Mass spectrometry data acquisition.** The MS datasets were acquired with two different
619 instrumental setups. The first setup (A) was utilized for the D1, Prod and NLS-GFP samples
620 from embryos, ovaries and testes. The second setup (B) was employed for acquiring the
621 Piwi and NLS-GFP samples from embryos. In setup A, LC-MS/MS acquisition was
622 performed on an Orbitrap QExactive+ mass spectrometer (ThermoFisher) coupled to an
623 EASY-nLC-1000 liquid chromatography system (ThermoFisher). Peptides were separated
624 using a reverse phase column (75µm ID x 400mm New Objective, in-house packed with
625 ReproSil Gold 120 C18, 1.9 µm, Dr. Maisch GmbH) across a gradient from 3 to 25% in 170
626 minutes and from 25 to 40% in 10 minutes (buffer A: 0.1% (v/v) formic acid; buffer B: 0.1%
627 (v/v) formic acid, 95% (v/v) acetonitrile). The DDA data acquisition mode was set to perform
628 one MS1 scan followed by a maximum of 20 scans for the top 20 most intense peptides
629 with MS1 scans (R=70'000 at 400m/z, AGC=1e6 and maximum IT=100 ms), HCD
630 fragmentation (NCE=25%), isolation windows (1.8 m/z) and MS2 scans (R=17'500 at
631 400m/z, AGC=1e5 and maximum IT=55ms). A dynamic exclusion of 30s was applied and
632 charge states lower than two and higher than seven were rejected for the isolation. In setup
633 B, LC-MS/MS acquisition was performed on an Orbitrap Exploris480 mass spectrometer
634 (ThermoFisher) coupled to an Vanquish Neo liquid chromatography system (ThermoFisher).
635 Peptides were separated using a reverse phase column (75µm ID x 400mm New Objective,

636 in-house packed with ReproSil Gold 120 C18, 1.9 µm, Dr. Maisch GmbH) across a linear
637 gradient from 7 to 35% in 120 minutes (buffer A: 0.1% (v/v) formic acid; buffer B: 0.1% (v/v)
638 formic acid, 95% (v/v) acetonitrile). The DDA data acquisition mode was set to perform one
639 MS1 scan followed by a maximum of 20 scans for the top 20 most intense peptides with
640 MS1 scans (R=60'000 at 400m/z, AGC=1e6 and auto maximum IT), HCD fragmentation
641 (NCE=28%), isolation windows (1.4 m/z) and MS2 scans (R=15'000 at 400m/z, AGC=2e5
642 and auto maximum IT). A dynamic exclusion of 25s was applied and charge states lower
643 than two and higher than six were rejected for the isolation.

644 **Mass spectrometry data analysis.** Acquired spectra were analyzed using the MaxQuant
645 software package version 1.5.2.8 embedded with the Andromeda search engine against
646 *Drosophila* proteome reference dataset (http://www.uniprot.org/, downloaded on
647 18.01.2021, 22'044 proteins including not reviewed proteins) extended with reverse decoy
648 sequences. The search parameters were set to include only full tryptic peptides, maximum
649 two missed cleavage, carbamidomethyl as static peptide modification, oxidation (M) and
650 deamidation (N-ter) as variable modification and "match between runs" option. The MS and
651 MS/MS mass tolerance was set to 10ppm. False discovery rate of <1% was used for
652 protein identification. Protein abundance was determined from the intensity of the top two
653 unique peptides. Intensity values were median normalized and imputed using random
654 sampling from a normal distribution-generated 1% less intense values. Statistical analysis
655 was performed using unpaired two-sided t-test. Hits identified from the differential analysis
656 between the bait pulldown versus the NLS-GFP control, with $\log_2$FC >1 and p-value < 0.05,
657 were considered as interacting proteins. Surprisingly, Prod spectra were not always reliably
658 identified in certain samples, even when used as bait. For pathway enrichment analysis, we
659 first generated a list of *Drosophila* DNA repair proteins (GO:0006281, Table S4) and a
660 custom list of transposon repression proteins based on the literature (Table S5) and used a

661 hypergeometric test to calculate the enrichment of proteins belonging to these lists in the
662 D1/Prod pulldowns.

663 **Structural predictions using Alphafold2.** To predict the structures of binary protein-protein
664 interactions, we used version 2.3.2 of Alphafold2, which contains updated parameters for
665 multimeric protein-protein interactions[44]. Default values for all parameters and for
666 generating multiple sequence alignments were used. To rank the models according to a
667 confidence metric, we used the ipTM score, which has been show to distinguish interacting
668 from non-interacting proteins[88]. Structural models are available upon request.
669

670 **Co-immunoprecipitation and western blotting.** For the co-immunoprecipitation, 125-
671 250mg of frozen embryos were thawed on ice and lysed in an identical manner to the ovary
672 lysis protocol detailed above. ~50μg of lysate was collected as input while ~970 μg of lysate
673 at a concentration of 2mg/ml was incubated with anti-GFP nanobody coupled beads (~ 50µl
674 slurry) (Chromotek AB_2631358) for 90 minutes at 4°C. After the incubation, beads were
675 washed three times for 5 minutes with a wash buffer (450 mM NaCl, 50mM Tris-HCl pH 7.5,
676 1mM MgCl2, 1 mM EDTA, 0.5mM DTT) at room temperature. Protein complexes bound to
677 the beads were eluted in 80μl of SDS sample buffer by heating at 95°C for 5 minutes. Input
678 samples were also brought to a final volume of 80μl by adding 30μl of SDS sample buffer.
679 Equal volumes of input and IP samples were loaded on a 4-12% SDS gradient gel (Sigma
680 Aldrich). Immunoprecipitated proteins were detected using mouse anti-GFP (1:1000, Roche
681 1181 4460001), guinea pig anti-D1 (1:1000, [26]) and rabbit anti-histone H3 (1:1000, Abcam
682 ab1791). Secondary antibodies used were Alexa Fluor Plus 800 donkey anti-mouse
683 (1:10,000, Invitrogen) and donkey anti-guinea pig IR dye 680 (1:10,000, Li-Cor). Western
684 blots were imaged using the Odyssey DLx fluorescence imager (Li-Cor).
685

686 **RNA sequencing and data analysis.** For each sample, approximately 5 pairs of ovaries
687 from 4 day old females were dissected in RNase-free 1x PBS and flash frozen in liquid
688 nitrogen until RNA extraction. RNA extraction for each replicate was performed using the
689 RNeasy RNA extraction kit (Qiagen). Samples were treated with DNase post RNA extraction
690 and purified using an RNA purification kit (Promega). RNA concentrations were assessed
691 using a Nanodrop as well as a Qubit RNA analyzer for sample quality and RIN scores.
692 rRNA-depleted libraries were prepared and sequenced by Novogene on an NovaSeq 6000
693 (Illumina) using paired-end 150 bp sequencing. The resulting raw reads were cleaned by
694 removing adaptor sequences, low-quality-end trimming, and removal of low-quality reads
695 using BBTools v 38.18 (Bushnell, B. *BBMap*. Available from:
696 https://sourceforge.net/projects/bbmap/). The exact commands used for quality control can
697 be found on the Methods in Microbiomics webpage (Sunagawa, S. *Data Preprocessing —*
698 *Methods in Microbiomics 0.0.1 documentation*. Available from: https://methods-in-
699 microbiomics.readthedocs.io/en/latest/preprocessing/preprocessing.html). The quality-
700 controlled reads were aligned against BDGP6.32 using STAR aligner[89]. Transcript and
701 transposon abundances were quantified using Tetranscripts[90]. Differential gene
702 expression analysis was performed using Bioconductor R package DESeq2 v 1.37.4[91].
703
704 **Small RNA sequencing and data analysis.** Small RNA cloning was performed as
705 previously described[75]. In brief, ~5 pairs of ovaries from three biological replicates per
706 genotype were lysed and Argonaute-sRNA complexes were isolated using TraPR ion
707 exchange spin columns. sRNAs were subsequently purified using acidic phenol. 3′ adaptors
708 containing six random nucleotides plus a 5 nt barcode on their 5′ end and 5′ adaptors
709 containing four random nucleotides at their 3′ end were subsequently ligated to the small
710 RNAs before reverse transcription, PCR amplification, and sequencing on an Illumina
711 NovaSeqSP instrument. Raw reads were trimmed for linker sequences, barcodes and the

712 4/6 random nucleotides before mapping to the *D. melanogaster* genome (dm6), using Bowtie
713 (version.1.3.0, settings: -f -v 3 -a --best --strata --sam) with 0 mismatches allowed. Genome-
714 mapping reads were crossreferenced with Flybase genome annotations (r6.40) using
715 BEDTools to allow the removal of reads mapping to rRNA, tRNA, snRNA, snoRNA loci, and
716 the mitochondrial genome. For TE mappings, all genome mappers were used allowing no
717 mismatches. Reads mapping to multiple elements were assigned to the best match. Reads
718 mapping equally well to multiple positions were randomly distributed. Libraries were
719 normalized to 1 million sequenced microRNA reads. For calculation of piRNAs mapping to
720 TEs, only antisense piRNAs were considered, and counts were normalized to TE length.
721
722 **Data Availability.** The mass spectrometry data have been deposited to the
723 ProteomeXchange Consortium via the PRIDE partner repository with the following dataset
724 identifiers: PXD044367 (IP-MS of D1 from Testis), PXD043237 (IP-MS of Piwi from Embryo),
725 PXD043236 (IP-MS of Prod and D1 in Ovary) and PXD043234 (IP-MS of Prod and D1 in
726 Embryo). We have also generated a web app to facilitate browsing of the proteomics data
727 (https://d1-prod-interactors-bcfffefc8a0d.herokuapp.com/).
728
729

730 **References**

731 1. Heitz E. Das Heterochromatin der Moose. I. Jb wiss Bot. 1928;69: 762–818.

732 2. Pardue ML, Gall JG. Chromosomal localization of mouse satellite DNA. Science.
733 1970;168: 1356–8.

734 3. Pimpinelli S, Berloco M, Fanti L, Dimitri P, Bonaccorsi S, Marchetti E, et al.
735 Transposable elements are stable structural components of Drosophila melanogaster
736 heterochromatin. Proc Natl Acad Sci U S A. 1995;92: 3804–8.

737 4. Kidwell MG, Kidwell JF, Sved JA. Hybrid Dysgenesis in DROSOPHILA
738 MELANOGASTER: A Syndrome of Aberrant Traits Including Mutation, Sterility and
739 Male Recombination. Genetics. 1977;86: 813–33.

740 5. Orsi GA, Joyce EF, Couble P, McKim KS, Loppin B. Drosophila I-R hybrid dysgenesis
741 is associated with catastrophic meiosis and abnormal zygote formation. Journal of Cell
742 Science. 2010;123: 3515–3524. doi:10.1242/jcs.073890

743 6. Zhu Q, Hoong N, Aslanian A, Hara T, Benner C, Heinz S, et al. Heterochromatin-
744 Encoded Satellite RNAs Induce Breast Cancer. Mol Cell. 2018;70: 842-853 e7.
745 doi:10.1016/j.molcel.2018.04.023

746 7. Ting DT, Lipson D, Paul S, Brannigan BW, Akhavanfard S, Coffman EJ, et al. Aberrant
747 Overexpression of Satellite Repeats in Pancreatic and Other Epithelial Cancers.
748 Science. 2011;331: 593–596. doi:10.1126/science.1200801

749 8. Mellone BG, Fachinetti D. Diverse mechanisms of centromere specification. Current
750 Biology. 2021;31: R1491–R1504. doi:10.1016/j.cub.2021.09.083

751 9. Kasinathan S, Henikoff S. Non-B-Form DNA Is Enriched at Centromeres. Mol Biol
752 Evol. 2018;35: 949–962. doi:10.1093/molbev/msy010

753 10. Dernburg AF, Sedat JW, Hawley RS. Direct Evidence of a Role for Heterochromatin in
754 Meiotic Chromosome Segregation. Cell. 1996;86: 135–146. doi:10.1016/S0092-
755 8674(00)80084-7

756 11. Dernburg AF, Broman KW, Fung JC, Marshall WF, Philips J, Agard DA, et al.
757 Perturbation of Nuclear Architecture by Long-Distance Chromosome Interactions. Cell.
758 1996;85: 745–759. doi:10.1016/S0092-8674(00)81240-4

759 12. Bouck DC, Bloom K. Pericentric Chromatin Is an Elastic Component of the Mitotic
760 Spindle. Current Biology. 2007;17: 741–748. doi:10.1016/j.cub.2007.03.033

761 13. Peters AH, O'Carroll D, Scherthan H, Mechtler K, Sauer S, Schofer C, et al. Loss of the
762 Suv39h histone methyltransferases impairs mammalian heterochromatin and genome
763 stability. Cell. 2001;107: 323–37.

764 14. Cosby RL, Chang N-C, Feschotte C. Host–transposon interactions: conflict,
765 cooperation, and cooption. Genes Dev. 2019;33: 1098–1116.
766 doi:10.1101/gad.327312.119

767 15. Cacchione S, Cenci G, Raffa GD. Silence at the End: How Drosophila Regulates
768 Expression and Transposition of Telomeric Retroelements. Journal of Molecular
769 Biology. 2020;432: 4305–4321. doi:10.1016/j.jmb.2020.06.004

770 16. Nelson JO, Slicko A, Yamashita YM. The retrotransposon R2 maintains Drosophila
771 ribosomal DNA repeats. Proceedings of the National Academy of Sciences. 2023;120:
772 e2221613120. doi:10.1073/pnas.2221613120

773 17. Chang C-H, Chavan A, Palladino J, Wei X, Martins NMC, Santinello B, et al. Islands of
774 retroelements are major components of Drosophila centromeres. Becker PB, editor.
775 PLoS Biol. 2019;17: e3000241. doi:10.1371/journal.pbio.3000241

776 18. Nowacki M, Higgins BP, Maquilan GM, Swart EC, Doak TG, Landweber LF. A
777 Functional Role for Transposases in a Large Eukaryotic Genome. Science. 2009;324:
778 935–938. doi:10.1126/science.1170023

779 19. Allshire RC, Madhani HD. Ten principles of heterochromatin formation and function.
780 Nat Rev Mol Cell Biol. 2018;19: 229–244. doi:10.1038/nrm.2017.119

781 20. Brändle F, Frühbauer B, Jagannathan M. Principles and functions of pericentromeric
782 satellite DNA clustering into chromocenters. Seminars in Cell & Developmental
783 Biology. 2022;128: 26–39. doi:10.1016/j.semcdb.2022.02.005

784 21. Seller CA, Cho C-Y, O'Farrell PH. Rapid embryonic cell cycles defer the establishment
785 of heterochromatin by Eggless/SetDB1 in Drosophila. Genes Dev. 2019;33: 403–417.
786 doi:10.1101/gad.321646.118

787 22. Yuan K, O'Farrell PH. TALE-light imaging reveals maternally guided, H3K9me2/3-
788 independent emergence of functional heterochromatin in Drosophila embryos. Genes
789 Dev. 2016;30: 579–593. doi:10.1101/gad.272237.115

790 23. Tang R, Zhou M, Chen Y, Jiang Z, Fan X, Zhang J, et al. H3K14ac facilitates the
791 reinstallation of constitutive heterochromatin in Drosophila early embryos by engaging
792 Eggless/SetDB1. Proceedings of the National Academy of Sciences. 2024;121:
793 e2321859121. doi:10.1073/pnas.2321859121

794 24. Atinbayeva N, Valent I, Zenk F, Loeser E, Rauer M, Herur S, et al. Inheritance of H3K9
795 methylation regulates genome architecture in Drosophila early embryos. The EMBO
796 Journal. 2024;43: 2685–2714. doi:10.1038/s44318-024-00127-z

797 25. Montavon T, Shukeir N, Erikson G, Engist B, Onishi-Seebacher M, Ryan D, et al.
798 Complete loss of H3K9 methylation dissolves mouse heterochromatin organization.
799 Nat Commun. 2021;12: 4359. doi:10.1038/s41467-021-24532-8

800 26. Jagannathan M, Cummings R, Yamashita YM. A conserved function for
801 pericentromeric satellite DNA. VijayRaghavan K, editor. eLife. 2018;7: e34122.
802 doi:10.7554/eLife.34122

803 27. Jagannathan M, Cummings R, Yamashita YM. The modular mechanism of
804 chromocenter formation in Drosophila. VijayRaghavan K, Gerbi SA, editors. eLife.
805 2019;8: e43938. doi:10.7554/eLife.43938

806 28. Alekseyenko AA, Gorchakov AA, Zee BM, Fuchs SM, Kharchenko PV, Kuroda MI.
807 Heterochromatin-associated interactions of *Drosophila* HP1a with dADD1, HIPP1, and
808 repetitive RNAs. Genes Dev. 2014;28: 1445–1460. doi:10.1101/gad.241950.114

809 29. Kochanova NY, Schauer T, Mathias GP, Lukacs A, Schmidt A, Flatley A, et al. A multi-
810 layered structure of the interphase chromocenter revealed by proximity-based
811 biotinylation. Nucleic Acids Research. 2020;48: 4161–4178. doi:10.1093/nar/gkaa145

812 30. Swenson JM, Colmenares SU, Strom AR, Costes SV, Karpen GH. The composition
813 and organization of Drosophila heterochromatin are heterogeneous and dynamic.
814 Shilatifard A, editor. eLife. 2016;5: e16096. doi:10.7554/eLife.16096

815 31. Thomae AW, Schade GOM, Padeken J, Borath M, Vetter I, Kremmer E, et al. A Pair of
816 Centromeric Proteins Mediates Reproductive Isolation in Drosophila Species.
817 Developmental Cell. 2013;27: 412–424. doi:10.1016/j.devcel.2013.10.001

818 32. Lukacs A, Thomae AW, Krueger P, Schauer T, Venkatasubramani AV, Kochanova NY,
819 et al. The Integrity of the Speciation Core Complex is necessary for centromeric
820 binding and reproductive isolation in Drosophila. bioRxiv. 2021; 2021.02.05.429932.
821 doi:10.1101/2021.02.05.429932

822 33. Torok T, Harvie PD, Buratovich M, Bryant PJ. The product of proliferation disrupter is
823 concentrated at centromeres and required for mitotic chromosome condensation and
824 cell proliferation in Drosophila. Genes & Development. 1997;11: 213–225.
825 doi:10.1101/gad.11.2.213

826 34. Schotta G, Ebert A, Krauss V, Fischer A, Hoffmann J, Rea S, et al. Central role of
827 Drosophila SU(VAR)3-9 in histone H3-K9 methylation and heterochromatic gene
828 silencing. EMBO J. 2002;21: 1121–1131. doi:10.1093/emboj/21.5.1121

829 35. Kerrebrock AW, Moore DP, Wu JS, Orr-Weaver TL. Mei-S332, a drosophila protein
830 required for sister-chromatid cohesion, can localize to meiotic centromere regions.
831 Cell. 1995;83: 247–256. doi:10.1016/0092-8674(95)90166-3

832 36. Satyaki PR, Cuykendall TN, Wei KH, Brideau NJ, Kwak H, Aruna S, et al. The Hmr and
833 Lhr hybrid incompatibility genes suppress a broad range of heterochromatic repeats.
834 PLoS Genet. 2014;10: e1004240. doi:10.1371/journal.pgen.1004240

835 37. Blum JA, Bonaccorsi S, Marzullo M, Palumbo V, Yamashita YM, Barbash DA, et al.
836 The Hybrid Incompatibility Genes Lhr and Hmr Are Required for Sister Chromatid
837 Detachment During Anaphase but Not for Centromere Function. Genetics. 2017;207:
838 1457–1472. doi:10.1534/genetics.117.300390

839 38. Ainsztein AM, Kandels-Lewis SE, Mackay AM, Earnshaw WC. INCENP Centromere
840 and Spindle Targeting: Identification of Essential Conserved Motifs and Involvement of
841 Heterochromatin Protein HP1. Journal of Cell Biology. 1998;143: 1763–1774.
842 doi:10.1083/jcb.143.7.1763

843 39. Reyes-Carmona S, Valadéz-Graham V, Aguilar-Fuentes J, Zurita M, León-Del-Río A.
844 Trafficking and chromatin dynamics of holocarboxylase synthetase during
845 development of Drosophila melanogaster. Molecular Genetics and Metabolism.
846 2011;103: 240–248. doi:10.1016/j.ymgme.2011.03.005

40. Huo X, Ji L, Zhang Y, Lv P, Cao X, Wang Q, et al. The Nuclear Matrix Protein SAFB Cooperates with Major Satellite RNAs to Stabilize Heterochromatin Architecture Partially through Phase Separation. Molecular Cell. 2020;77: 368-383.e7. doi:10.1016/j.molcel.2019.10.001

41. Guruharsha KG, Rual JF, Zhai B, Mintseris J, Vaidya P, Vaidya N, et al. A protein complex network of Drosophila melanogaster. Cell. 2011;147: 690–703. doi:10.1016/j.cell.2011.08.047

42. Tang H-W, Spirohn K, Hu Y, Hao T, Kovács IA, Gao Y, et al. Next-generation large-scale binary protein interaction network for Drosophila melanogaster. Nat Commun. 2023;14: 2162. doi:10.1038/s41467-023-37876-0

43. Szklarczyk D, Kirsch R, Koutrouli M, Nastou K, Mehryary F, Hachilif R, et al. The STRING database in 2023: protein-protein association networks and functional enrichment analyses for any sequenced genome of interest. Nucleic Acids Res. 2023;51: D638–D646. doi:10.1093/nar/gkac1000

44. Evans R, O'Neill M, Pritzel A, Antropova N, Senior A, Green T, et al. Protein complex prediction with AlphaFold-Multimer. bioRxiv; 2022. p. 2021.10.04.463034. doi:10.1101/2021.10.04.463034

45. Durham J, Zhang J, Humphreys IR, Pei J, Cong Q. Recent advances in predicting and modeling protein–protein interactions. Trends in Biochemical Sciences. 2023;48: 527–538. doi:10.1016/j.tibs.2023.03.003

46. Burke DF, Bryant P, Barrio-Hernandez I, Memon D, Pozzati G, Shenoy A, et al. Towards a structurally resolved human protein interaction network. Nat Struct Mol Biol. 2023;30: 216–225. doi:10.1038/s41594-022-00910-8

47. Kim A-R, Hu Y, Comjean A, Rodiger J, Mohr SE, Perrimon N. Enhanced Protein-Protein Interaction Discovery via AlphaFold-Multimer. bioRxiv; 2024. p. 2024.02.19.580970. doi:10.1101/2024.02.19.580970

48. Charlesworth B, Sniegowski P, Stephan W. The evolutionary dynamics of repetitive DNA in eukaryotes. Nature. 1994;371: 215–220. doi:10.1038/371215a0

49. Chiolo I, Minoda A, Colmenares SU, Polyzos A, Costes SV, Karpen GH. Double-strand breaks in heterochromatin move outside of a dynamic HP1a domain to complete recombinational repair. Cell. 2011;144: 732–744. doi:10.1016/j.cell.2011.02.012

50. Ryu T, Spatola B, Delabaere L, Bowlin K, Hopp H, Kunitake R, et al. Heterochromatic breaks move to the nuclear periphery to continue recombinational repair. Nat Cell Biol. 2015;17: 1401–1411. doi:10.1038/ncb3258

51. Mitrentsi I, Lou J, Kerjouan A, Verigos J, Reina-San-Martin B, Hinde E, et al. Heterochromatic repeat clustering imposes a physical barrier on homologous recombination to prevent chromosomal translocations. Molecular Cell. 2022;82: 2132-2147.e6. doi:10.1016/j.molcel.2022.03.033

52. Hughes SE, Hawley RS. Topoisomerase II Is Required for the Proper Separation of Heterochromatic Regions during Drosophila melanogaster Female Meiosis. PLOS Genetics. 2014;10: e1004650. doi:10.1371/journal.pgen.1004650

53. Caridi CP, D'Agostino C, Ryu T, Zapotoczny G, Delabaere L, Li X, et al. Nuclear F-actin and myosins drive relocalization of heterochromatic breaks. Nature. 2018;559: 54–60. doi:10.1038/s41586-018-0242-8

54. Bourque G, Burns KH, Gehring M, Gorbunova V, Seluanov A, Hammell M, et al. Ten things you should know about transposable elements. Genome Biology. 2018;19: 199. doi:10.1186/s13059-018-1577-z

55. Ozata DM, Gainetdinov I, Zoch A, O'Carroll D, Zamore PD. PIWI-interacting RNAs: small RNAs with big functions. Nat Rev Genet. 2019;20: 89–108. doi:10.1038/s41576-018-0073-3

56. Czech B, Munafò M, Ciabrelli F, Eastwood EL, Fabry MH, Kneuss E, et al. piRNA-Guided Genome Defense: From Biogenesis to Silencing. Annual Review of Genetics. 2018;52: 131–157. doi:10.1146/annurev-genet-120417-031441

57. Klattenhoff C, Xi H, Li C, Lee S, Xu J, Khurana JS, et al. The Drosophila HP1 Homolog Rhino Is Required for Transposon Silencing and piRNA Production by Dual-Strand Clusters. Cell. 2009;138: 1137–1149. doi:10.1016/j.cell.2009.07.014

58. Zhang Z, Wang J, Schultz N, Zhang F, Parhad SS, Tu S, et al. The HP1 Homolog Rhino Anchors a Nuclear Complex that Suppresses piRNA Precursor Splicing. Cell. 2014;157: 1353–1363. doi:10.1016/j.cell.2014.04.030

59. Mohn F, Sienski G, Handler D, Brennecke J. The Rhino-Deadlock-Cutoff Complex Licenses Noncanonical Transcription of Dual-Strand piRNA Clusters in Drosophila. Cell. 2014;157: 1364–1379. doi:10.1016/j.cell.2014.04.031

60. Andreev VI, Yu C, Wang J, Schnabl J, Tirian L, Gehre M, et al. Panoramix SUMOylation on chromatin connects the piRNA pathway to the cellular heterochromatin machinery. Nat Struct Mol Biol. 2022;29: 130–142. doi:10.1038/s41594-022-00721-x

61. Jankovics F, Bence M, Sinka R, Faragó A, Bodai L, Pettkó-Szandtner A, et al. Drosophila small ovary gene is required for transposon silencing and heterochromatin organization, and ensures germline stem cell maintenance and differentiation. Development. 2018;145: dev170639. doi:10.1242/dev.170639

62. Benner L, Castro EA, Whitworth C, Venken KJT, Yang H, Fang J, et al. Drosophila Heterochromatin Stabilization Requires the Zinc-Finger Protein Small Ovary. Genetics. 2019;213: 877–895. doi:10.1534/genetics.119.302590

63. Onishi R, Sato K, Murano K, Negishi L, Siomi H, Siomi MC. Piwi suppresses transcription of Brahma-dependent transposons via Maelstrom in ovarian somatic cells. Science Advances. 2020;6: eaaz7420. doi:10.1126/sciadv.aaz7420

64. Sun J, Liu C, Bai X, Li X, Li J, Zhang Z, et al. Drosophila FIT is a protein-specific satiety hormone essential for feeding control. Nat Commun. 2017;8: 14161. doi:10.1038/ncomms14161

65. Wei X, Eickbush DG, Speece I, Larracuente AM. Heterochromatin-dependent transcription of satellite DNAs in the Drosophila melanogaster female germline. Weigel D, editor. eLife. 2021;10: e62375. doi:10.7554/eLife.62375

929 66. Giauque CC, Bickel SE. Heterochromatin-Associated Proteins HP1a and Piwi
930 Collaborate to Maintain the Association of Achiasmate Homologs in Drosophila
931 Oocytes. Genetics. 2016;203: 173–189. doi:10.1534/genetics.115.186460

932 67. Brower-Toland B, Findley SD, Jiang L, Liu L, Yin H, Dus M, et al. Drosophila PIWI
933 associates with chromatin and interacts directly with HP1a. Genes Dev. 2007;21:
934 2300–2311. doi:10.1101/gad.1564307

935 68. Gu T, Elgin SCR. Maternal Depletion of Piwi, a Component of the RNAi System,
936 Impacts Heterochromatin Formation in Drosophila. PLOS Genetics. 2013;9: e1003780.
937 doi:10.1371/journal.pgen.1003780

938 69. Ma X, Wang S, Do T, Song X, Inaba M, Nishimoto Y, et al. Piwi Is Required in Multiple
939 Cell Types to Control Germline Stem Cell Lineage Development in the Drosophila
940 Ovary. PLOS ONE. 2014;9: e90267. doi:10.1371/journal.pone.0090267

941 70. Handler D, Meixner K, Pizka M, Lauss K, Schmied C, Gruber FS, et al. The Genetic
942 Makeup of the Drosophila piRNA Pathway. Molecular Cell. 2013;50: 762–777.
943 doi:10.1016/j.molcel.2013.04.031

944 71. Czech B, Preall JB, McGinn J, Hannon GJ. A Transcriptome-wide RNAi Screen in the
945 Drosophila Ovary Reveals Factors of the Germline piRNA Pathway. Molecular Cell.
946 2013;50: 749–761. doi:10.1016/j.molcel.2013.04.007

947 72. Ghabrial A, Schüpbach T. Activation of a meiotic checkpoint regulates translation of
948 Gurken during Drosophila oogenesis. Nat Cell Biol. 1999;1: 354–357.
949 doi:10.1038/14046

950 73. Moon S, Cassani M, Lin YA, Wang L, Dou K, Zhang ZZ. A Robust Transposon-
951 Endogenizing Response from Germline Stem Cells. Dev Cell. 2018;47: 660-671 e3.
952 doi:10.1016/j.devcel.2018.10.011

953 74. Sienski G, Dönertas D, Brennecke J. Transcriptional Silencing of Transposons by Piwi
954 and Maelstrom and Its Impact on Chromatin State and Gene Expression. Cell.
955 2012;151: 964–980. doi:10.1016/j.cell.2012.10.040

956 75. Baumgartner L, Handler D, Platzer SW, Yu C, Duchek P, Brennecke J. The Drosophila
957 ZAD zinc finger protein Kipferl guides Rhino to piRNA clusters. Bourc'his D, Struhl K,
958 Zhang Z, editors. eLife. 2022;11: e80067. doi:10.7554/eLife.80067

959 76. Kneuss E, Munafò M, Eastwood EL, Deumer U-S, Preall JB, Hannon GJ, et al.
960 Specialization of the *Drosophila* nuclear export family protein Nxf3 for piRNA precursor
961 export. Genes Dev. 2019;33: 1208–1220. doi:10.1101/gad.328690.119

962 77. ElMaghraby MF, Andersen PR, Pühringer F, Hohmann U, Meixner K, Lendl T, et al. A
963 Heterochromatin-Specific RNA Export Pathway Facilitates piRNA Production. Cell.
964 2019;178: 964-979.e20. doi:10.1016/j.cell.2019.07.007

965 78. Staller MV, Yan D, Randklev S, Bragdon MD, Wunderlich ZB, Tao R, et al. Depleting
966 Gene Activities in Early Drosophila Embryos with the "Maternal-Gal4–shRNA" System.
967 Genetics. 2013;193: 51–61. doi:10.1534/genetics.112.144915

79. Lin H, Spradling AC. A novel group of pumilio mutations affects the asymmetric division of germline stem cells in the Drosophila ovary. Development. 1997;124: 2463–2476. doi:10.1242/dev.124.12.2463

80. Sun X, Wahlstrom J, Karpen G. Molecular structure of a functional Drosophila centromere. Cell. 1997;91: 1007–19.

81. Fabry MH, Falconio FA, Joud F, Lythgoe EK, Czech B, Hannon GJ. Maternally inherited piRNAs direct transient heterochromatin formation at active transposons during early Drosophila embryogenesis. Struhl K, editor. eLife. 2021;10: e68573. doi:10.7554/eLife.68573

82. Gonzalez LE, Tang X, Lin H. Maternal Piwi regulates primordial germ cell development to ensure the fertility of female progeny in Drosophila. Genetics. 2021;219: iyab091. doi:10.1093/genetics/iyab091

83. Erdel F. Phase transitions in heterochromatin organization. Current Opinion in Structural Biology. 2023;80: 102597. doi:10.1016/j.sbi.2023.102597

84. Van Doren M, Williamson AL, Lehmann R. Regulation of zygotic gene expression in Drosophilaprimordialgerm cells. Current Biology. 1998;8: 243–246. doi:10.1016/S0960-9822(98)70091-0

85. Zeidler MP, Perrimon N, Strutt DI. Polarity determination in the Drosophila eye: a novel role for Unpaired and JAK/STAT signaling. Genes Dev. 1999;13: 1342–1353.

86. Lu KL, Nelson JO, Watase GJ, Warsinger-Pepe N, Yamashita YM. Transgenerational dynamics of rDNA copy number in Drosophila male germline stem cells. Spradling AC, editor. eLife. 2018;7: e32421. doi:10.7554/eLife.32421

87. Wiśniewski JR, Zougman A, Nagaraj N, Mann M. Universal sample preparation method for proteome analysis. Nat Methods. 2009;6: 359–362. doi:10.1038/nmeth.1322

88. Bryant P, Pozzati G, Elofsson A. Improved prediction of protein-protein interactions using AlphaFold2. Nat Commun. 2022;13: 1265. doi:10.1038/s41467-022-28865-w

89. Dobin A, Davis CA, Schlesinger F, Drenkow J, Zaleski C, Jha S, et al. STAR: ultrafast universal RNA-seq aligner. Bioinformatics. 2013;29: 15–21. doi:10.1093/bioinformatics/bts635

90. Jin Y, Tam OH, Paniagua E, Hammell M. TEtranscripts: a package for including transposable elements in differential expression analysis of RNA-seq datasets. Bioinformatics. 2015;31: 3593–3599. doi:10.1093/bioinformatics/btv422

91. Love MI, Huber W, Anders S. Moderated estimation of fold change and dispersion for RNA-seq data with DESeq2. Genome Biology. 2014;15: 550. doi:10.1186/s13059-014-0550-8

Acknowledgements

We thank members of the Jagannathan lab, Ulrike Kutay, Ruth Kroschewski and Hugo Stocker for discussion and comments on the manuscript. We thank Benjamin Frühbauer for help with representing the protein models. We thank Daniel Barbash, Ferenc Jankovics, Yukiko Yamashita, the Bloomington Drosophila Stock Center, the Vienna Drosophila Resource Center, the Kyoto Drosophila Stock Center and the Developmental Studies Hybridoma Bank for reagents and resources. We thank the Scientific Center for optical and Electron Microscopy (ScopeM) and the Mass Spectrometry facility at the Institute of Biochemistry at ETH Zurich for technical support. We thank Shinichi Sunagawa for providing bioinformatics resources. M.J is supported by a project grant (310030_189131) from the Swiss National Science Foundation. A.C acknowledges support from Genetics Society of America in the form of a DeLill Nasser Award for Professional Development in Genetics.

1019 **Figures and Legends**

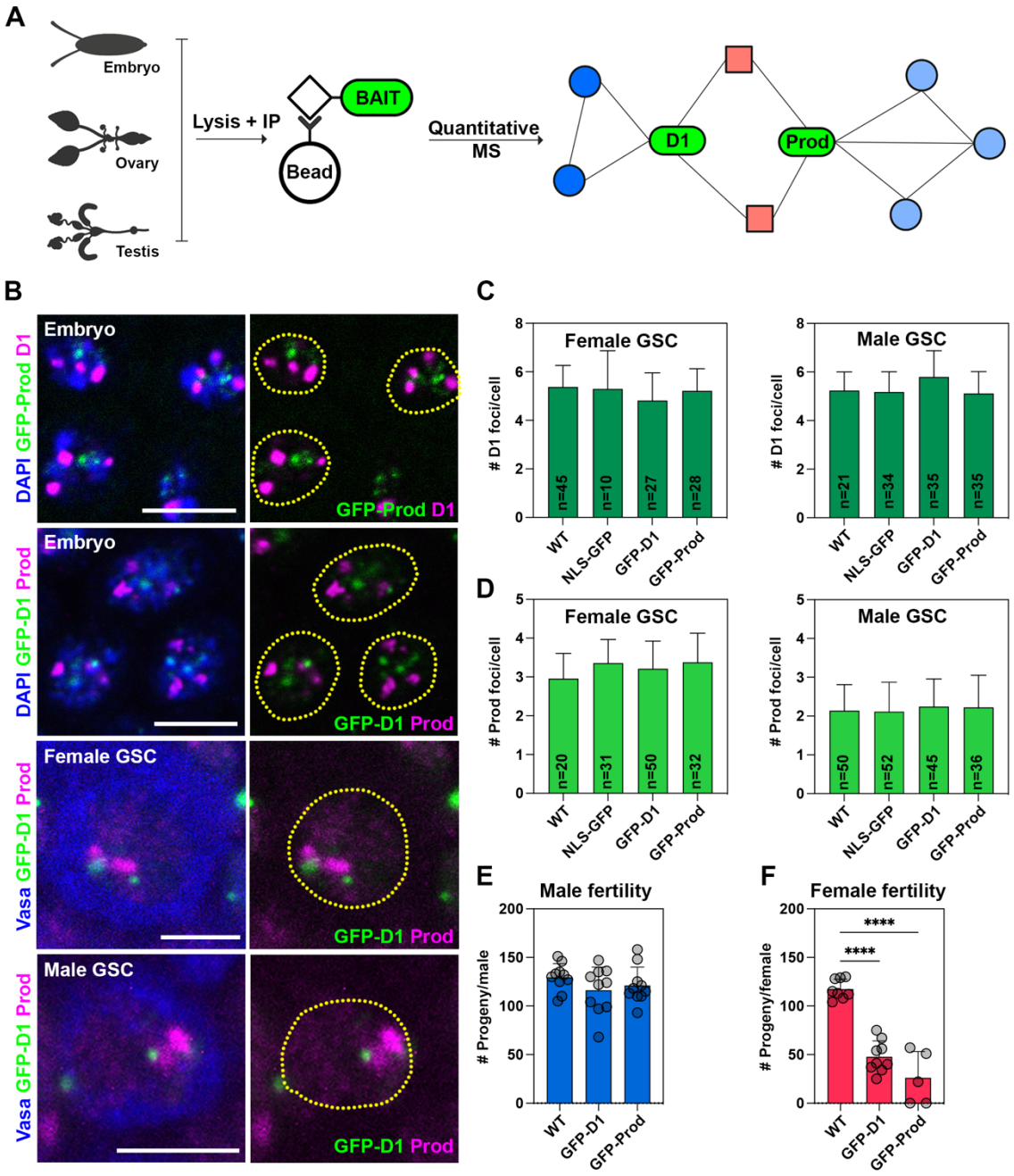

1020

1021 **Figure 1. Experimental setup for the characterization of the chromocenter-associated**

1022 **proteome.** (A) Experimental scheme for the identification of D1- and Prod-associated

1023 proteins across multiple *Drosophila* tissues using quantitative mass spectrometry. (B) D1

1024 and Prod are in proximity within the nucleus in multiple cell types including gastrulating

1025 embryos, female germ cells and male germ cells. (C) Bar plot of the total number of D1 foci

1026 present in female GSCs and male GSCs in the wild type (*yw*), *NLS-GFP*, *GFP-D1* and *GFP-*

1027 *Prod* strains. n indicates the number of cells analyzed. (D) Bar plot of the total number of
1028 Prod foci present in female GSCs and male GSCs in the wild type (*yw*), *NLS-GFP*, *GFP-D1*
1029 and *GFP-Prod* strains. n indicates the number of cells analyzed. (E, F) Bar plot of the
1030 number of progeny sired by a single tester male (E) or female (F) when mated with two wild
1031 type flies of the opposite sex over the course of one week. **** represents $p<0.0001$ from an
1032 ordinary one-way ANOVA. All error bars are SD and all scale bars are 5μm.

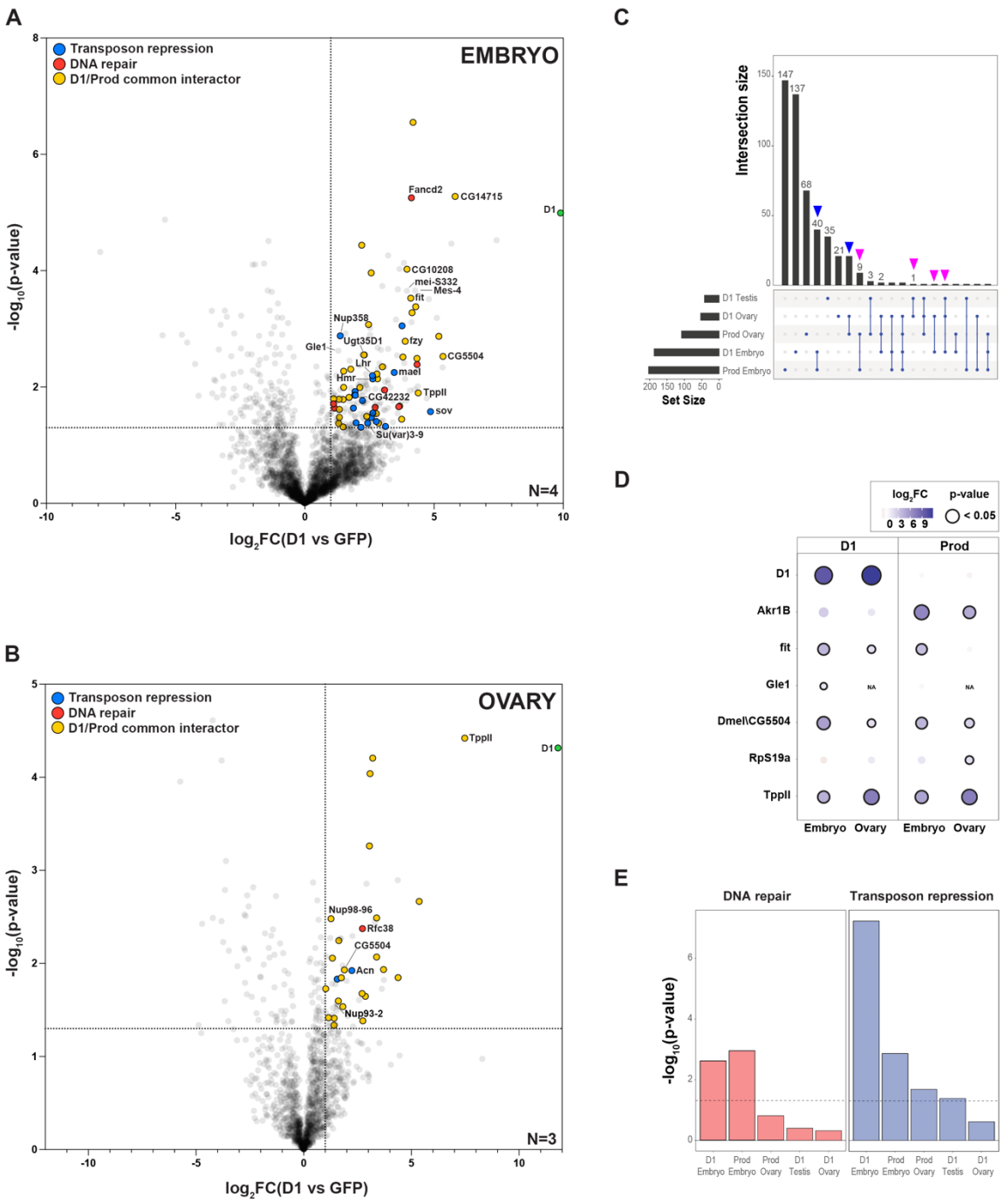

1033

1034 **Figure 2. The chromocenter-associated proteome across *Drosophila* tissues.** (A-B)

1035 Volcano plots of the D1-associated proteome in embryos (A) and ovaries (B). The dashed

1036 lines mark $\log_2$FC>1 and p<0.05; blue points indicate proteins involved in transposon

1037 repression, red points indicate proteins involved in DNA repair and yellow points indicate

1038 proteins pulled down by D1 and Prod. Number of biological replicates are indicated in the

1039 plot. (C) Intersection plot representing number of overlapping proteins in the D1 and Prod
1040 pulldowns from different tissues. Blue arrowheads indicate number of proteins common to
1041 D1 and Prod pulldown in the same tissue while magenta arrowheads indicate number of
1042 common proteins pulled down by D1 or Prod across different tissues (D) Enrichment of the
1043 selected proteins pulled down by D1 and Prod from more than one tissue. The size and
1044 colour of the circles are proportional to the log_2FC while the black outline indicates $p<0.05$.
1045 (E) Hypergeometric test of DNA repair or transposon repression pathway proteins from the
1046 multi-tissue D1 and Prod interactome. Dashed line indicates $p=0.05$.

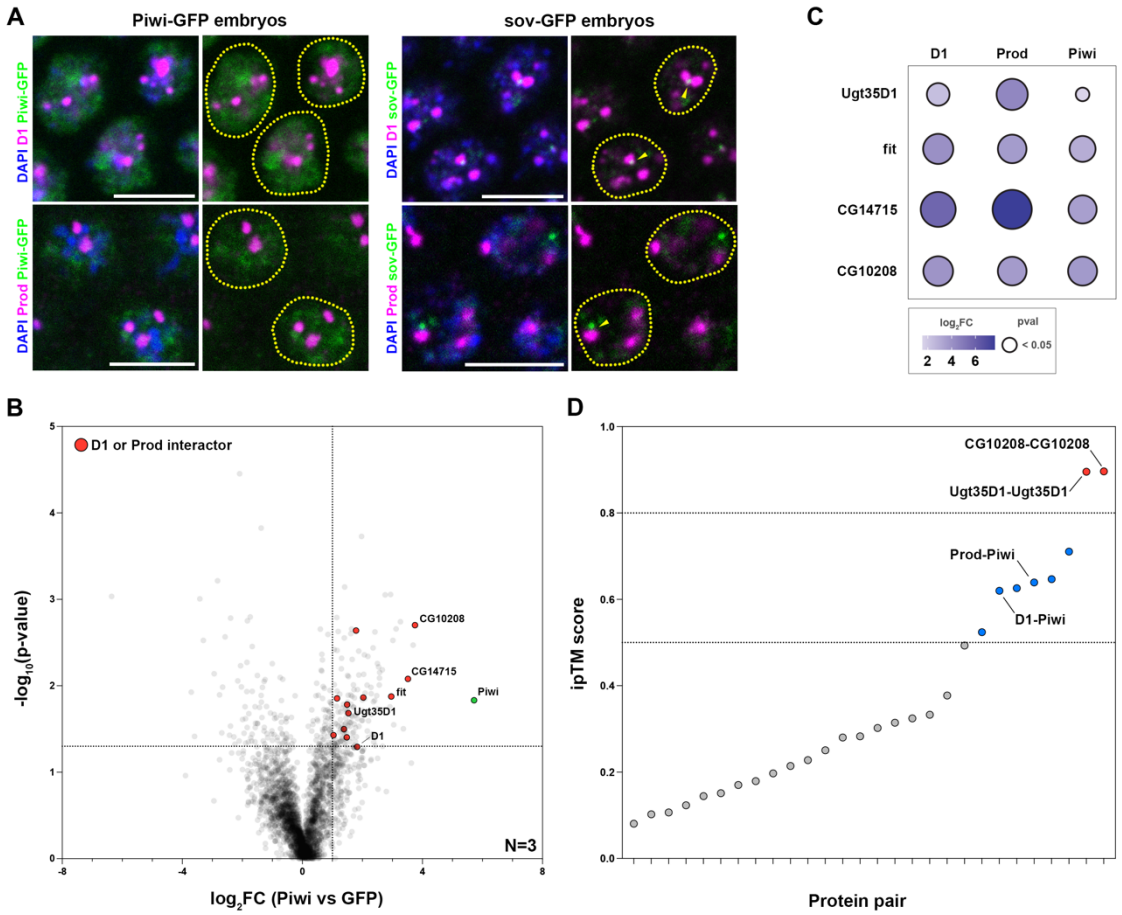

Figure 3. Molecular relationships between proteins involved in transposon repression and chromocenter formation (A) GFP-Piwi and Sov-GFP embryos were stained with D1/Prod (magenta) and DAPI (blue). Arrowheads indicate Sov-GFP foci in proximity to chromocenter boundaries. (B) Volcano plot of the Piwi-associated proteome in embryos. The dashed lines mark $\log_2FC>1$ and $p<0.05$ while the red points indicate proteins identified in pulldowns of D1 or Prod from embryos. Number of biological replicates are indicated. (C) Enrichment of the selected proteins pulled down by D1, Prod and Piwi from embryos. The size and colour of the circles are proportional to the $\log_2FC$ while the black outline indicates $p<0.05$. (D) ipTM scores of the pairwise protein structural models based on Alphafold Multimer. Gray points indicate low confidence structural models, blue points indicate medium confidence structural models (ipTM>0.5) and red points indicate high confidence structural models (ipTM>0.8). All scale bars are 5μm.

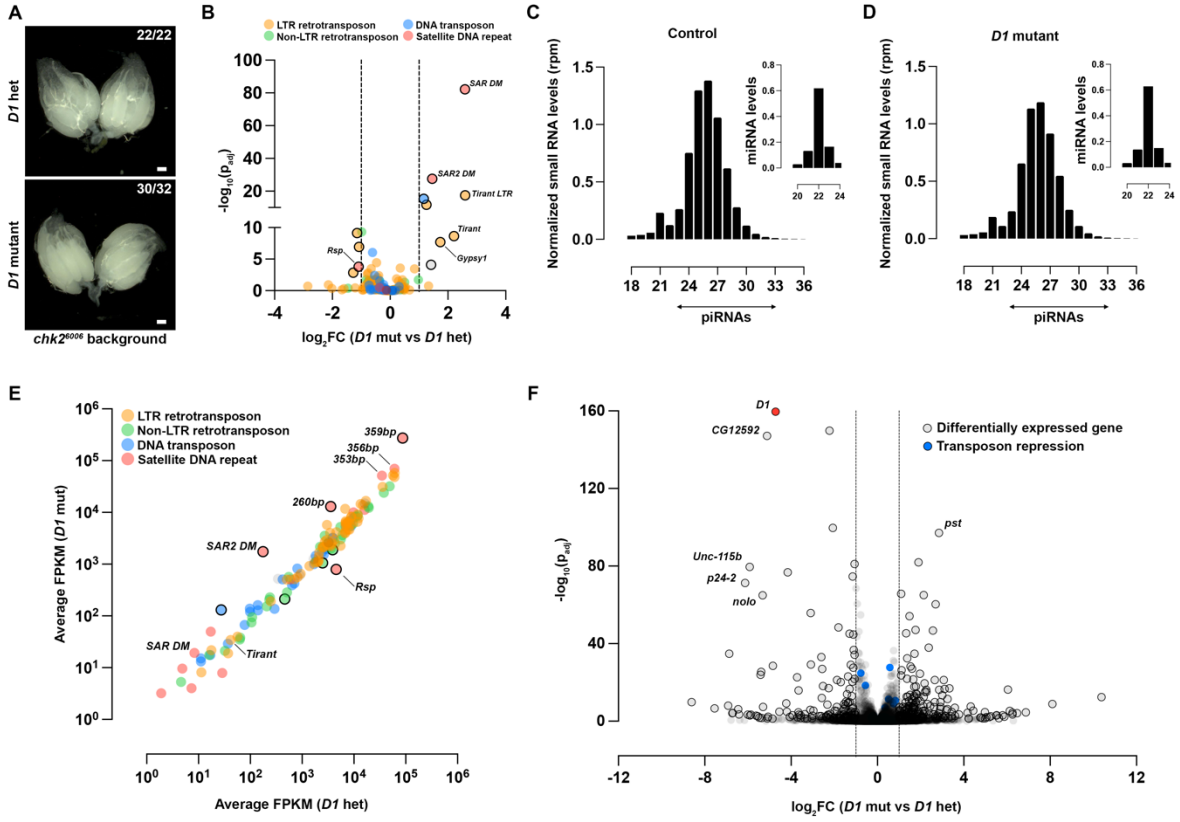

Figure 4. The effect of D1 on piRNA biogenesis and TE expression in ovaries. (A) Brightfield images of ovaries from *D1* heterozygous and *D1* mutant females in a *chk2*^{6006} background. Scale bars: 100µm. (B) Volcano plot of differentially expressed transposon families in ovaries from *D1* heterozygous and *D1* mutant females in a *chk2*^{6006} background (n=3). Statistically significant changes ($\log_2$FC >1, p_{adj} <0.05) are indicated with the black outlines. (C, D) Size profiles of Argonaute-bound small RNAs and miRNAs isolated from *D1* heterozygous and *D1* mutant ovaries. Reads from three replicates per genotype were normalized per million miRNA reads. (E) Average FPKM for piRNAs mapping antisense to transposon consensus sequences from D1 heterozygous and D1 mutant ovaries (n=3). Black outline indicates statistically significant changes in antisense piRNAs ($\log_2$FC >1, p_{adj}<0.05) (F) Volcano plot of differentially expressed genes in ovaries from *D1* heterozygous and *D1* mutant females in a *chk2*^{6006} background (n=3). Statistically significant changes ($\log_2$FC >1, p_{adj} <0.05) are indicated with the black outlines. Blue points indicate the 347 genes associated with transposon repression (Table S6).

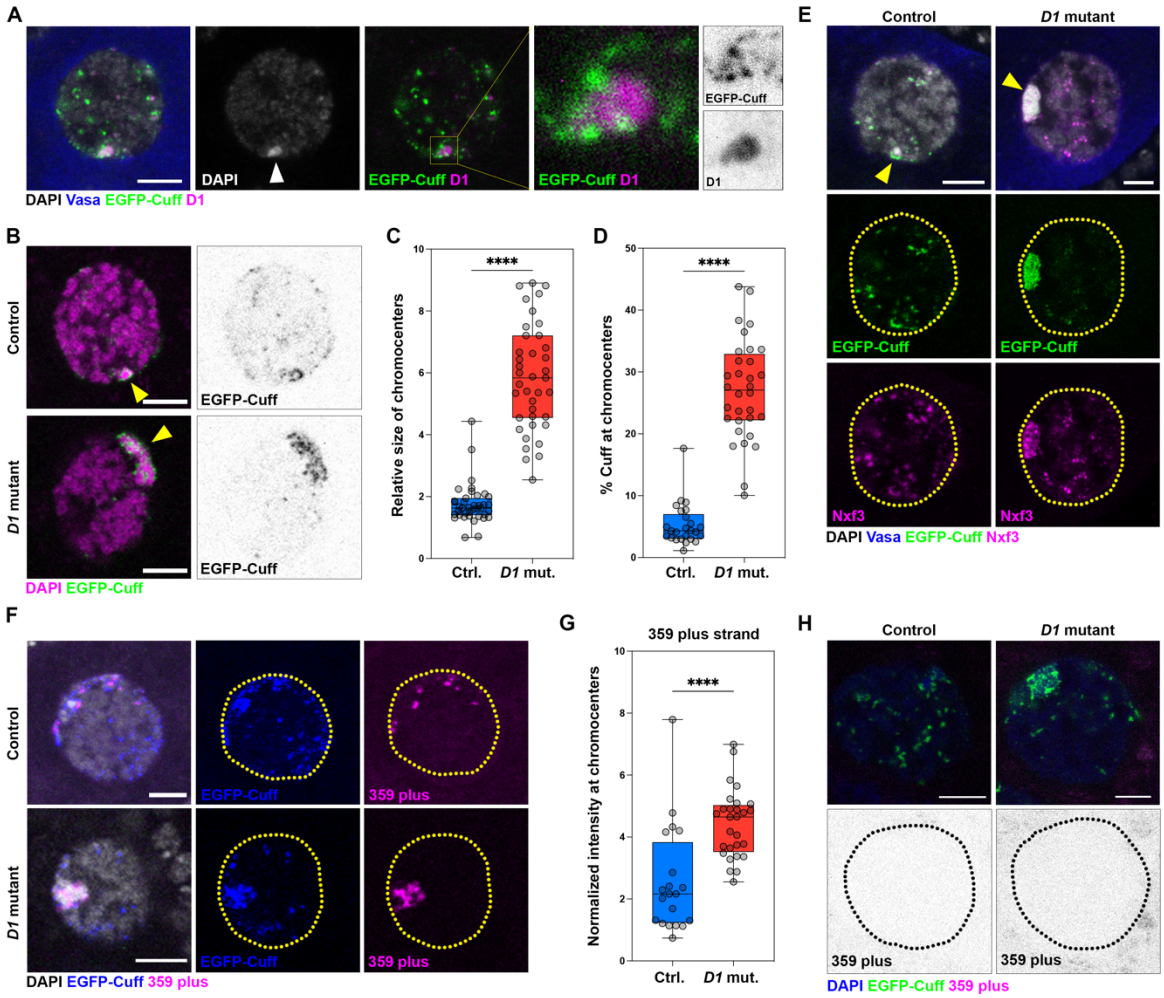

Figure 5. D1 blocks localization of the piRNA biogenesis machinery to chromocenters. (A) A single nurse cell from an EGFP-Cuff ovary stained with D1 (magenta), Vasa (blue) and DAPI (gray). The arrowhead points to the DAPI-dense chromocenter. The insets highlight Cuff localization at the periphery of D1-containing chromocenters. (B) Localization of EGFP-Cuff in nurse cell nuclei from control ($D1^{LL03310}$/TM6C) and D1 mutant ($D1^{LL03310}/Df(3R)^{Bsc666}$) ovaries. Yellow arrowheads point to the location of the chromocenter. (C) Box-and-whisker plot of the size of nurse cell chromocenters relative to total nuclear size in control ($D1^{LL03310}$/TM6C) and D1 mutant ($D1^{LL03310}/Df(3R)^{Bsc666}$) ovaries. **** represents p<0.0001 from a student's t-test. (D) Box-and-whisker plot of EGFP-Cuff enrichment at chromocenters relative to the rest of the nurse cell nucleus in control ($D1^{LL03310}$/TM6C) and D1 mutant ($D1^{LL03310}/Df(3R)^{Bsc666}$) ovaries. **** represents p<0.0001 from a student's t-test. (E) Localization of EGFP-Cuff (green) and Nxf3 (magenta) in nurse cell nuclei from control

1088 ($D1^{LL03310}$/TM6C) and D1 mutant ($D1^{LL03310}/Df(3R)^{Bsc666}$) ovaries. Yellow arrowheads point to

1089 the location of the chromocenter. (F) RNA *in situ* hybridization against the 359bp satellite

1090 DNA transcripts (plus strand, magenta) in control ($D1^{LL03310}$/TM6C) and D1 mutant

1091 ($D1^{LL03310}/Df(3R)^{Bsc666}$) ovaries in an EGFP-Cuff (blue) background that were also stained for

1092 DAPI (grey). (G) Box-and-whisker plot of chromocenter-localized 359bp satellite DNA

1093 transcripts in nurse cells from control ($D1^{LL03310}$/TM6C) and D1 mutant ($D1^{LL03310}/Df(3R)^{Bsc666}$)

1094 ovaries in an EGFP-Cuff background. **** represents $p<0.0001$ from a student's t-test. All

1095 scale bars are 5μm. (H) RNA *in situ* hybridization against the 359bp satellite DNA transcripts

1096 (plus strand, magenta) in control ($D1^{LL03310}$/TM6C) and D1 mutant ($D1^{LL03310}/Df(3R)^{Bsc666}$)

1097 ovaries in an EGFP-Cuff (green) background that were also stained for DAPI (blue) following

1098 RNase A treatment post fixation.

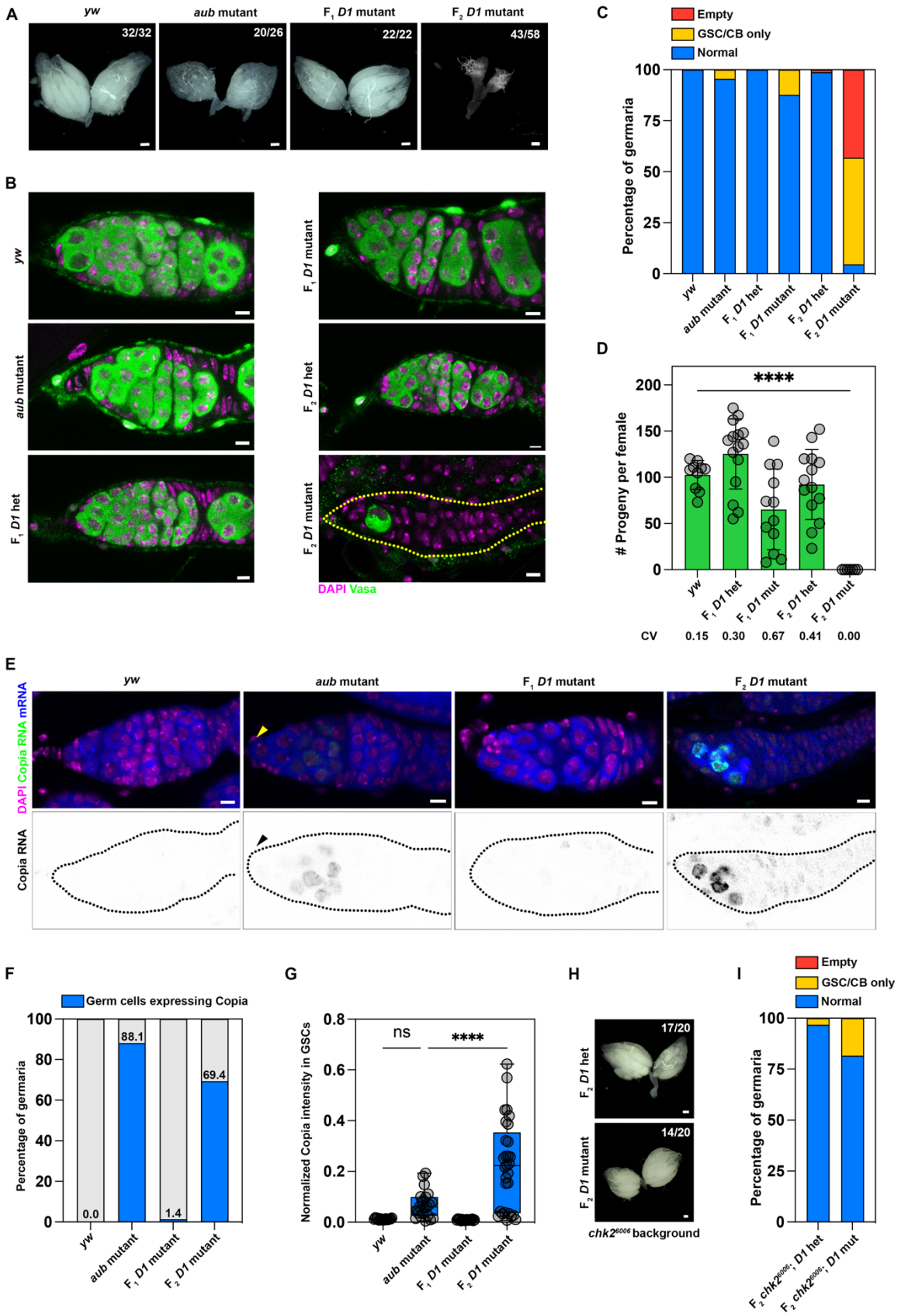
A
yw
aub mutant
F1 D1 mutant
F2 D1 mutant
32/32
20/26
22/22
43/58
B
yw
aub mutant
F1 D1 het
F1 D1 mutant
F2 D1 het
F2 D1 mutant
DAPI Vasa
C
Empty
GSC/CB only
Normal
Percentage of germaria
100
75
50
25
0
yw
aub mutant
F1 D1 het
F1 D1 mutant
F2 D1 het
F2 D1 mutant
D
****
Progeny per female
200
150
100
50
0
yw
F1 D1 het
F1 D1 mut
F2 D1 het
F2 D1 mut
CV
0.15
0.30
0.67
0.41
0.00
E
yw
aub mutant
F1 D1 mutant
F2 D1 mutant
DAPI Copia RNA mRNA
Copia RNA
F
Germ cells expressing Copia
Percentage of germaria
100
80
60
40
20
0
0.0
88.1
1.4
69.4
yw
aub mutant
F1 D1 mutant
F2 D1 mutant
G
ns
****
Normalized Copia intensity in GSCs
0.8
0.6
0.4
0.2
0.0
yw
aub mutant
F1 D1 mutant
F2 D1 mutant
H
F2 D1 het
F2 D1 mutant
17/20
14/20
chk2 6006 background
I
Empty
GSC/CB only
Normal
Percentage of germaria
100
75
50
25
0
F2 chk2 6006; D1 het
F2 chk2 6006; D1 mut

1099

1100 **Figure 6. Loss of D1 during embryogenesis triggers transposon expression in adult**
1101 **ovaries.** (A) Brightfield images of ovaries from the indicated genotypes. Scale bars: 100μm.
1102 (B) Ovaries from the indicated genotypes were stained with Vasa (green) and DAPI
1103 (magenta). Scale bars: 5μm. (C) Percentage of germaria containing a normal population of
1104 germ cells, only germline stem cells/cystoblasts (GSC/CB only) or completely lacking germ
1105 cells in *yw* (n=48), *aubergine* mutant (n=66), F_1 *D1* heterozygous (n=51), F_1 *D1* mutant
1106 (n=65), F_2 *D1* heterozygous (n=81) and F_2 *D1* mutant (n=109). (D) Bar plot of the number of
1107 progeny sired by a single female of the indicated genotypes when mated with two wild type
1108 males over the course of one week. CV represents coefficient of variation. **** represents
1109 $p<0.0001$ from an ordinary one-way ANOVA. (E) RNA *in situ* hybridization against Copia
1110 (green) and total polyadenylated mRNA (blue) was performed in ovaries of the indicated
1111 genotypes that were also stained for DAPI (magenta). Yellow and black arrowheads indicate
1112 undifferentiated germ cells in the *aubergine* mutant germarium. Scale bars: 5μm. (F)
1113 Percentage of germaria with germ cells expressing Copia transcripts in *yw* (n=62),
1114 *aubergine* mutant (n=67), F_1 *D1* mutant (n=71) and F_2 *D1* mutant (n=50). (G) Box-and-
1115 whisker plot of copia expression normalized to total polyA mRNA in undifferentiated germ
1116 cells (GSCs/CBs) from *yw* (n=16), *aubergine* mutant (n=22), F_1 *D1* mutant (n=18) and F_2 *D1*
1117 mutant (n=29). **** represents $p<0.0001$ from one-way ANOVA. (H) Brightfield images of
1118 ovaries from the indicated genotypes. Scale bars: 100μm. (I) Percentage of germaria
1119 containing a normal population of germ cells, only germline stem cells/cystoblasts (GSC/CB
1120 only) or completely lacking germ cells in F_2 *D1* heterozygous (n=62) and F_2 *D1* mutant
1121 (n=38) ovaries in a *Chk2* mutant background.

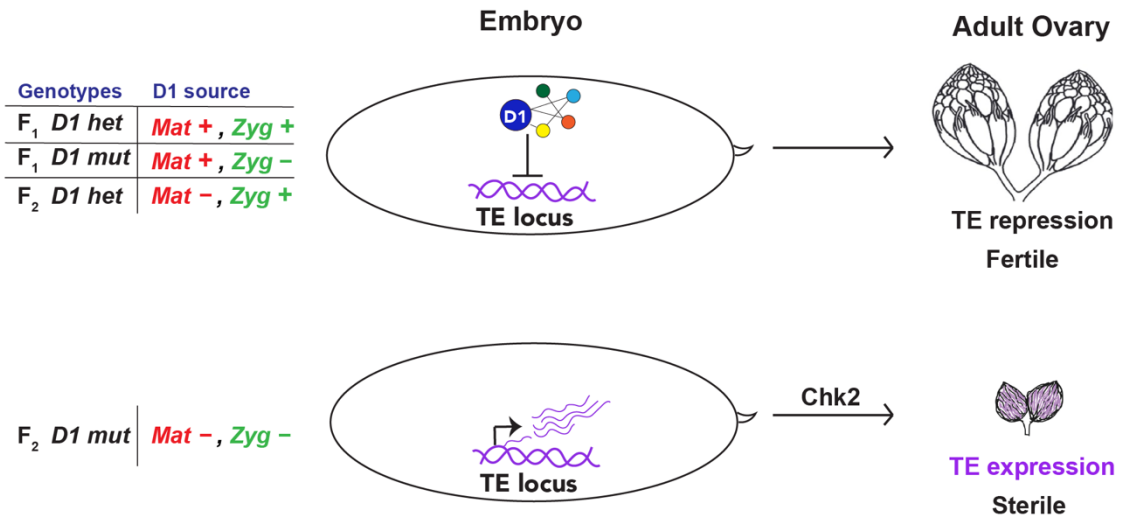

Figure 7. The role of D1 in heritable TE repression. An embryonic pool of D1 that originates from either maternal deposition (*Mat* +) and/or zygotic expression (*Zyg* +) is important for TE repression in adult gonads. In the absence of embryonic D1 (F_2 *D1* mt, *Mat* – *Zyg* –), TE expression contributes to Chk2-mediated gonadal atrophy.

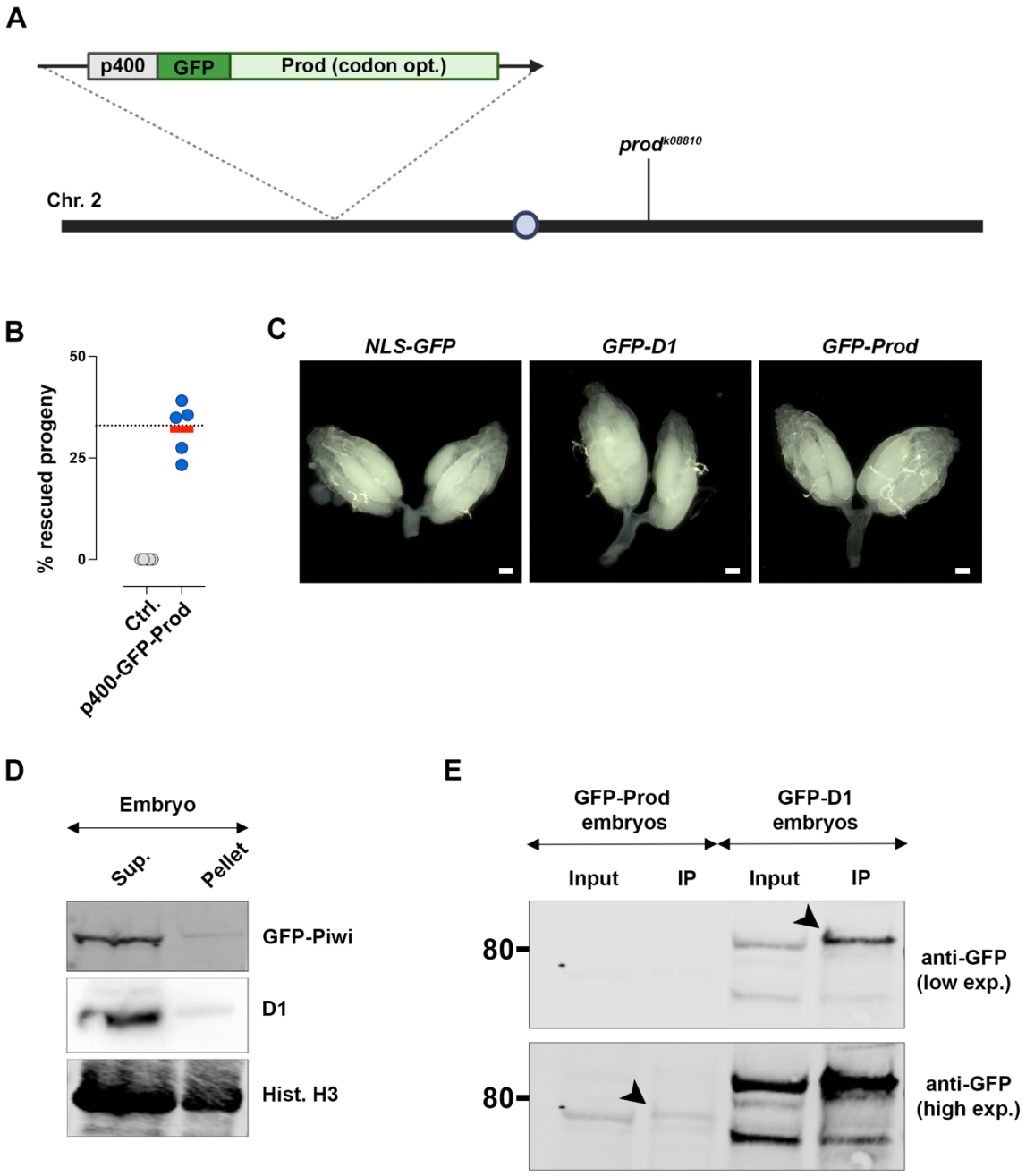

1127

1128 **Supplementary Figure 1. Schematic of the GFP-Prod allele and optimization of sample**

1129 **lysis and immunoprecipitation.** (A) A 400bp promoter sequence upstream of the Prod

1130 translation start site was placed upstream of a GFP-tagged and codon-optimized Prod

1131 sequence, inserted into the attP40 locus and recombined with the *prod*^{k08810} loss-of-

1132 function allele. (B) Rescue of prod mutant (*prod*$^{k08810/U}$) lethality was assessed using p400-

1133 GFP-Prod, *prod*^{k08810} (p400-GFP-Prod, 447 flies were counted from 5 crosses) and *prod*^{k08810}

1134 (Ctrl, 314 flies were counted from 5 crosses). Red line indicates median while dashed line
1135 indicates percent progeny for complete rescue. (C) Brightfield images of ovaries from the
1136 indicated genotypes. Scale bars: 100μm. (D) Western blot of equivalent fractions of the
1137 soluble supernatant and insoluble pellet from GFP-Piwi embryos using mouse anti-GFP,
1138 guinea pig anti-D1 and rabbit anti-H3 (loading control). (E) Immunoprecipitation of GFP from
1139 embryos expressing GFP-Prod or GFP-D1. Immunoprecipitated proteins were blotted using
1140 mouse anti-GFP and are indicated by arrowheads. Expected sizes: GFP-Prod: 75kDa, GFP-
1141 D1: 80kDa.
1142

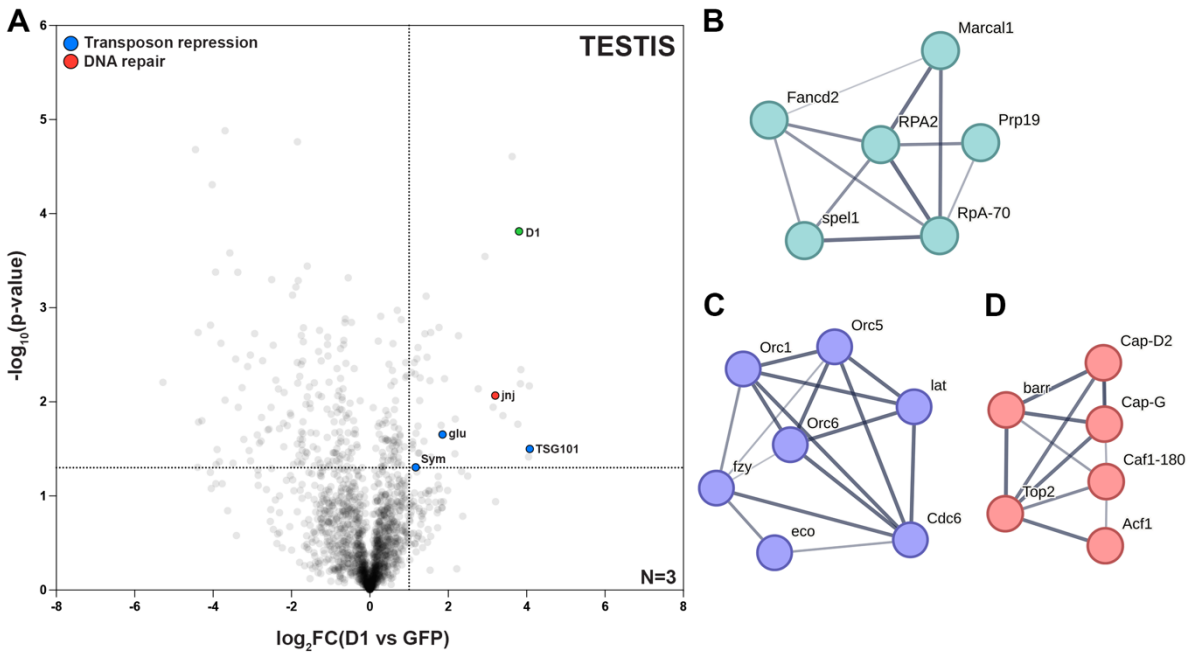

Supplementary Figure 2. Characterization of D1- and Prod-associated proteins in GSC-enriched testes and embryos. (A) Volcano plot of the D1-associated proteome in GSC-enriched testes. The dashed lines mark $\log_2FC>1$ and $p<0.05$; blue points indicate proteins involved in transposon repression and red points indicate proteins involved in DNA repair. Number of biological replicates are indicated in the plot. (B-D) k-means clustering of embryo hits using STRING-DB show relationships between Prod-associated (B) and D1-associated (C, D) proteins.

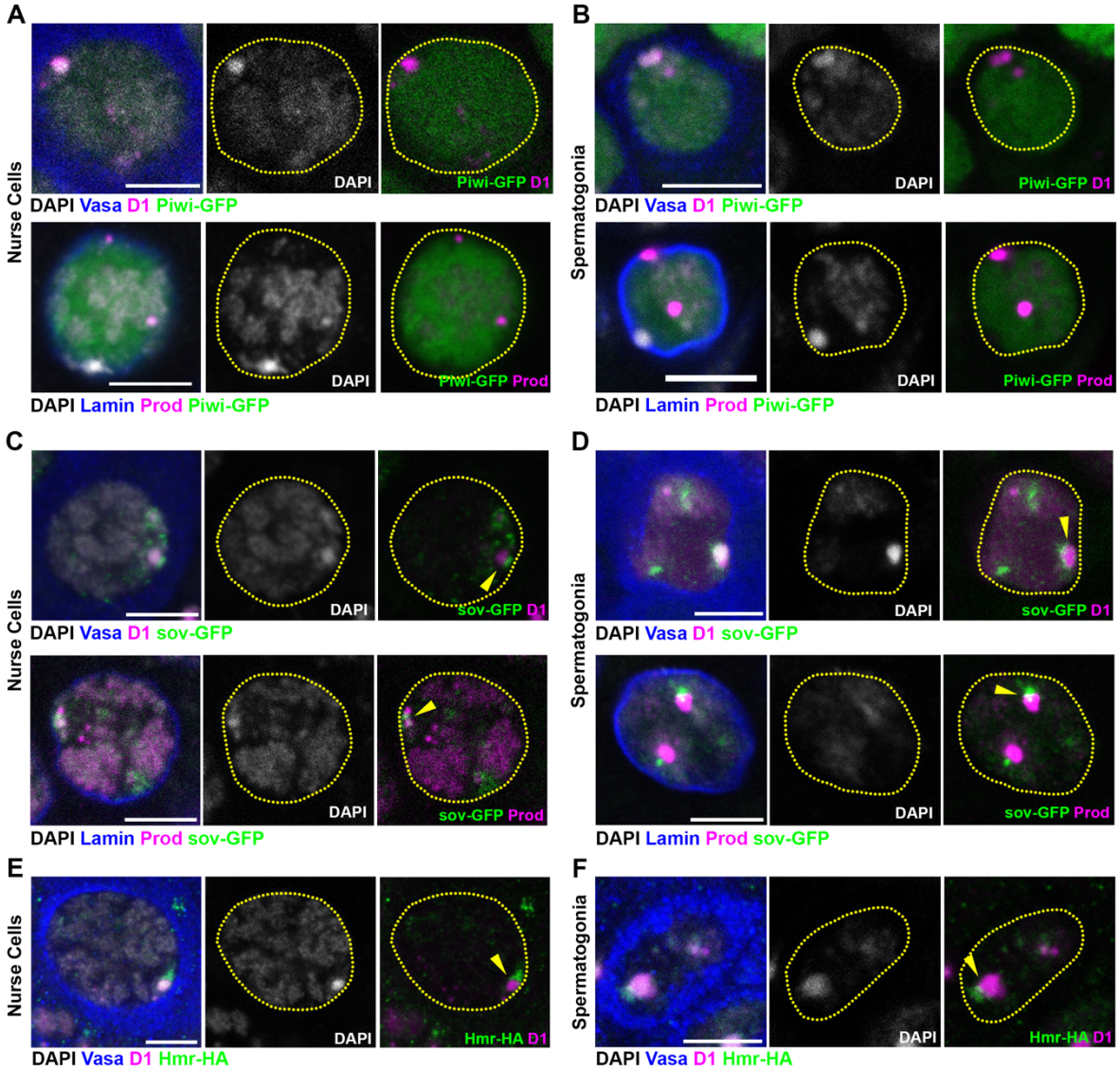

Supplementary Figure 3. Localization of D1 and Prod with respect to Piwi, Sov and Hmr in nurse cells and spermatogonia. GFP-Piwi (A, B), sov-GFP (C, D) and Hmr-HA (E, F) ovaries and testes were stained with D1/Prod (magenta), Vasa/Lamin (blue) and DAPI (gray). Arrowheads indicate sov or Hmr foci in proximity to chromocenter boundaries in individual nurse cells or spermatogonia. Scale bars: 5μm.

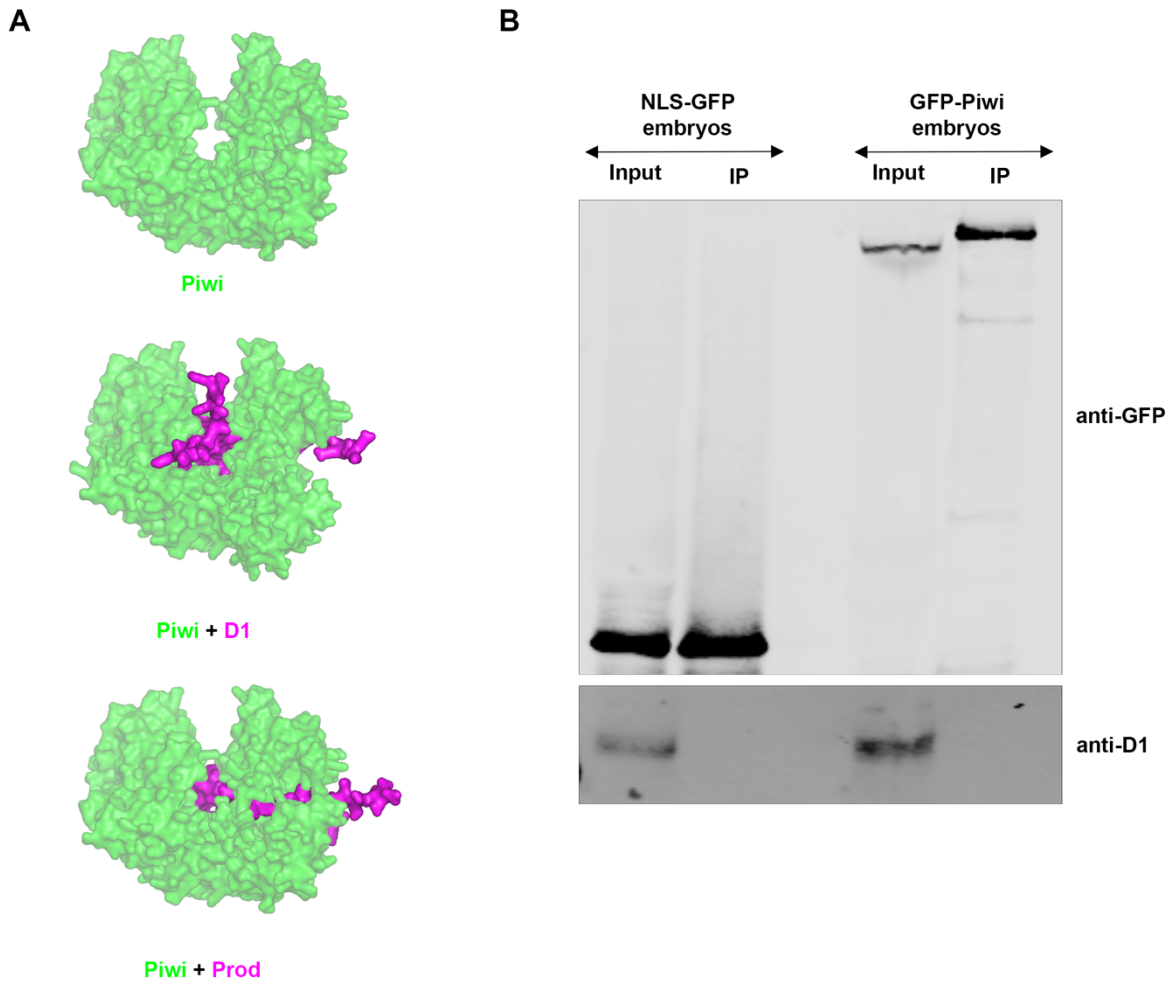

1157

1158 **Supplementary Figure 4. Assessing the interactions between Piwi and satellite DNA-**

1159 **binding proteins by AFM structural modelling and co-immunoprecipitation.** (A)

1160 Representation of the D1-Piwi and D1-Prod interaction interfaces predicted by Alphafold

1161 Multimer structural modelling. The following regions on D1 (120-143, 157-175 and 322-355)

1162 and on Prod (120-181 and 320-343) are depicted in magenta. (B) Immunoprecipitation of

1163 GFP and Piwi using GFP-trap beads from NLS-GFP (control) and GFP-Piwi embryos.

1164 Immunoprecipitated proteins were blotted using mouse anti-GFP and guinea pig anti-D1.

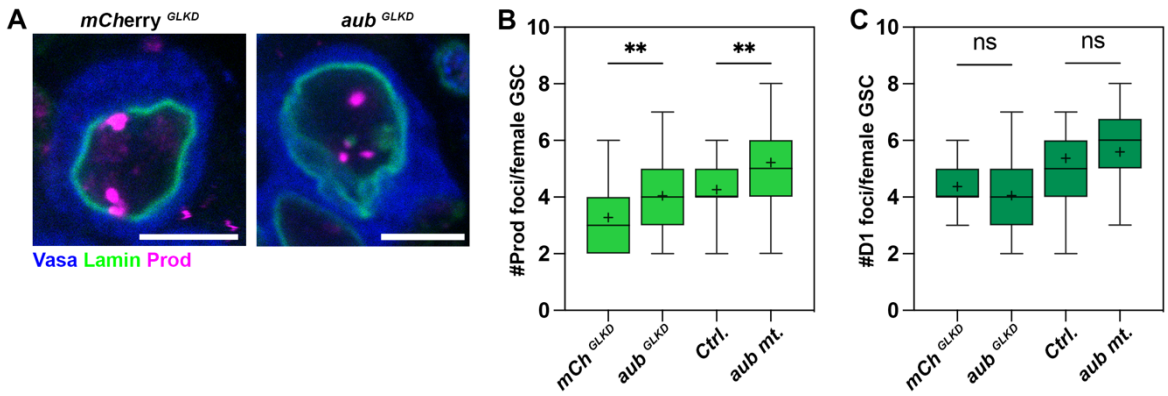

Supplementary Figure 5. Loss of *aubergine* has a mild effect on Prod foci in female GSCs. (A) Female GSCs expressing *mCherry*^{RNAi} (*mCherry*^{GLKD}) or *aub*^{RNAi} (*aub*^{GLKD}) under the control of *nos-gal4* stained for Prod (magenta), Lamin (green) and Vasa (blue). Scale bars: 5μm. (B, C) Box-and-whisker plot of the total number of Prod foci (B) or D1 foci (C) present per female GSC in *mCherry*^{GLKD} (n=58 for Prod, n=60 for D1), *aub*^{GLKD} (n=42 for Prod, n=36 for D1), *aubergine* heterozygous control (Ctrl., n=38 for Prod, n=59 for D1) and *aubergine* mutant (*aub*$^{QC42/HN2}$, n=52 for Prod, n=56 for D1). n indicates the number of cells analyzed. ** indicates $p<0.01$ based on a one-way ANOVA.

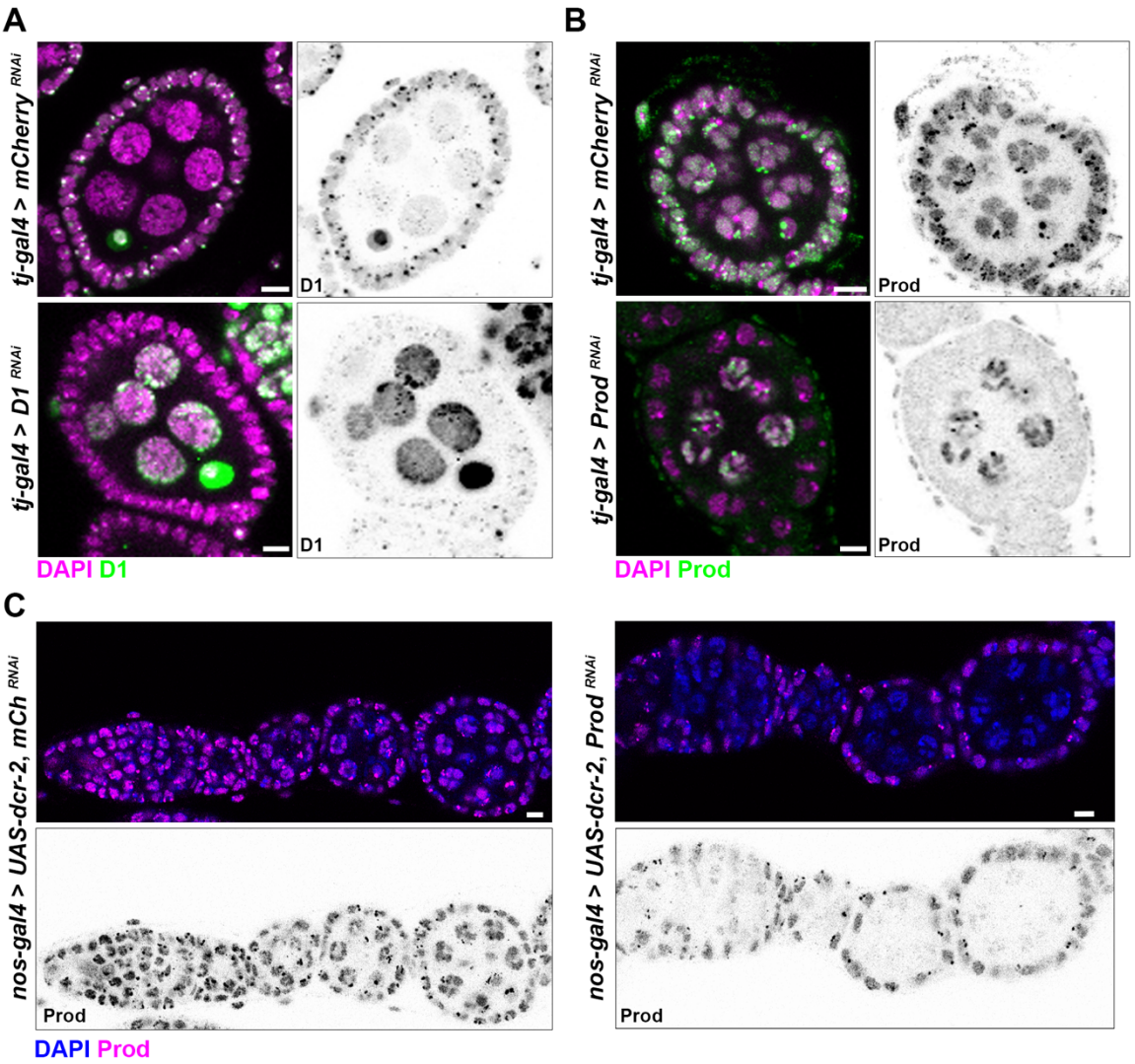

1174

1175 **Supplementary Figure 6. Validation of D1 and Prod knockdowns in gonadal somatic**

1176 **cells and germline cells.** (A, B) Individual egg chambers stained for DAPI (magenta) and

1177 Prod/D1 following *tj-gal4* mediated expression of *D1* ^{RNAi} (KK110307) or *Prod* ^{RNAi}

1178 (KK104361). *mCherry* ^{RNAi} was used as a control. (C, D) Anterior region of individual

1179 ovarioles were stained for DAPI (blue) and Prod (magenta) following *nos-gal4* mediated

1180 expression of *mCherry* ^{RNAi} (C) or *Prod* ^{RNAi} (D). Scale bars: 5μm.

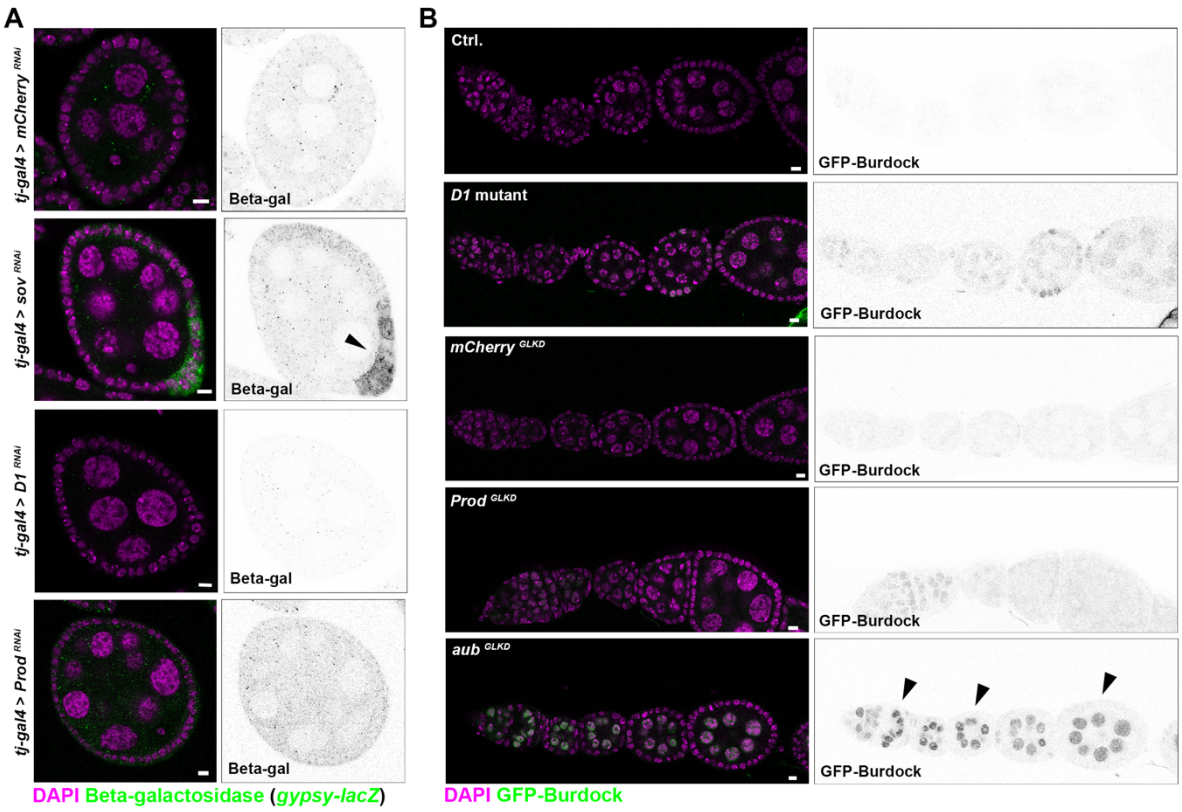

Supplementary Figure 7. Loss of D1 or Prod does not trigger expression of transposon reporters in gonadal somatic cells or germ cells. (A) Individual egg chambers stained for beta-galactosidase (indicating expression of *gypsy-lacZ*) following *tj-gal4* mediated expression of *mCherry* ^{RNAi}, *sov* ^{RNAi} (HMC04875), *D1* ^{RNAi} (KK110307) or *Prod* ^{RNAi} (KK104361). Arrowhead indicates follicle cells expressing *gypsy-lacZ*. (B) Anterior region of individual ovarioles were stained for DAPI in the following strains carrying GFP-Burdock-lacZ: *D1*^{LL03310}/*TM6B* (Ctrl.) and *D1*^{LL03310}/*Df(3R)*^{Bsc666} (*D1* mutant), *nos* > *mCherry* ^{RNAi} (*mCherry* ^{GLKD}), *nos* > *Prod* ^{RNAi} (*Prod* ^{GLKD}), *nos* > *aub*^{RNAi} (HMS01945, *aub* ^{GLKD}). Arrowheads indicate germ cells expressing GFP-Burdock. Scale bars: 5μm.

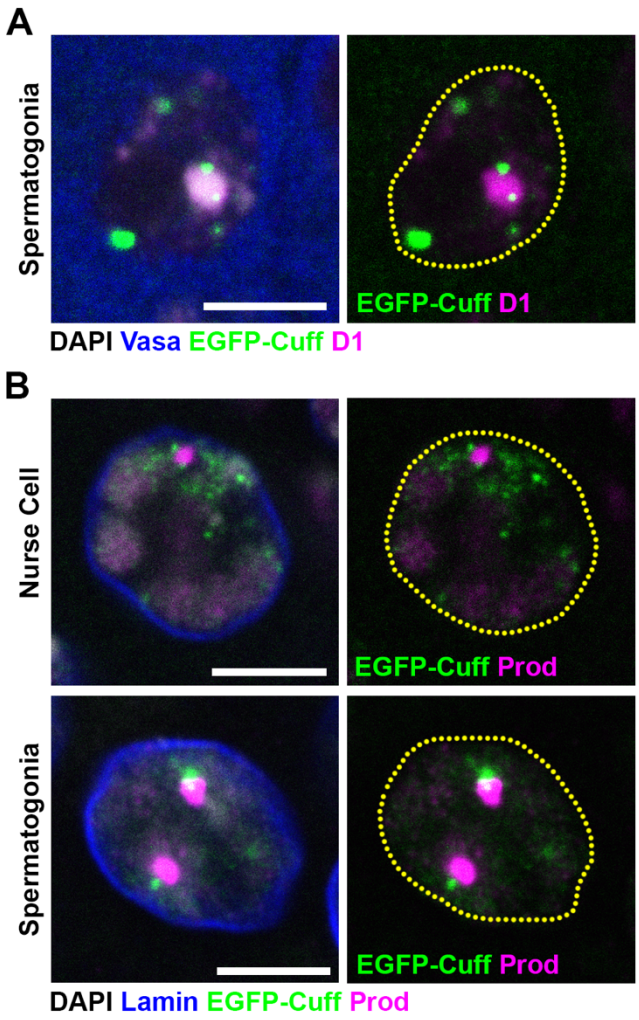

1191

1192 **Supplementary Figure 8. Localization of EGFP-Cuff relative to chromocenters.** (A, B)

1193 EGFP-Cuff ovaries and testes were stained for D1/Prod (magenta), Vasa/Lamin (blue) and

1194 DAPI (gray). Individual nurse cells or spermatogonia are depicted. Scale bars: 5μm.

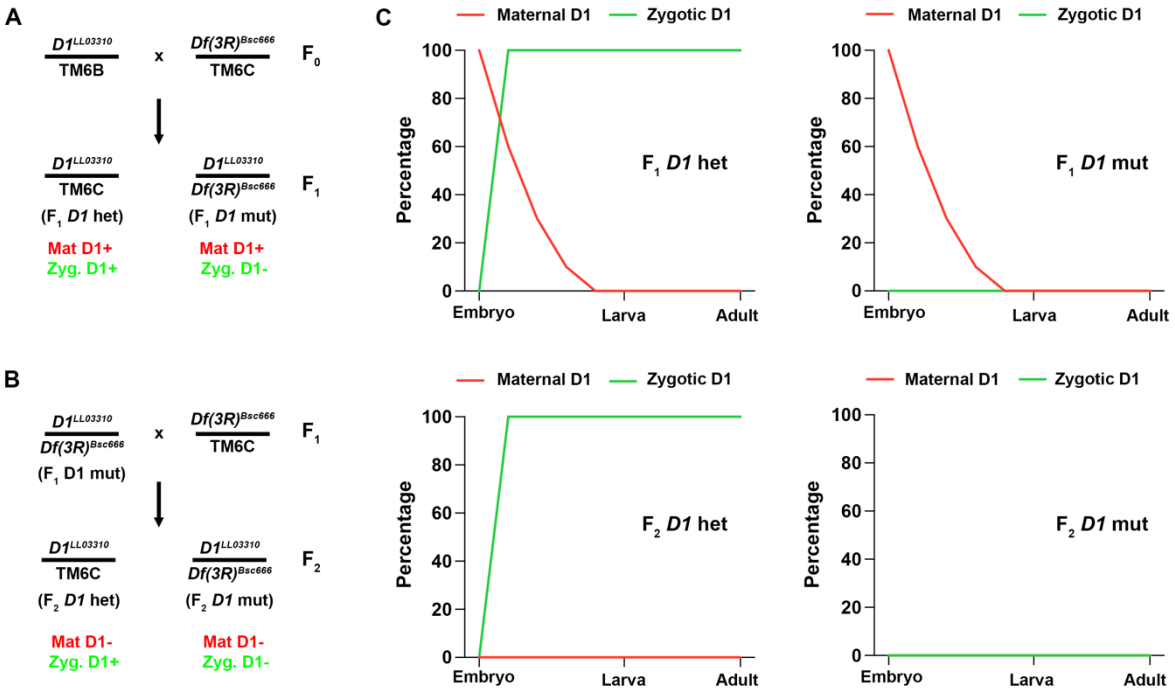

Supplementary Figure 9. Putative expression levels of maternal and zygotic D1 through development. (A, B) Crossing schemes used to generate F_1 *D1* mutants and F_2 *D1* mutants. (C) Theoretical depiction of maternal deposition and zygotic expression of D1 across embryonic, larval and adult stages in the indicated genotypes.

1200 **Supplementary Tables**

1201

1202 **Supplementary Table 1. List of proteins detected by LC-MS/MS in embryonic lysates**
1203 **from GFP-D1, GFP-Prod and NLS-GFP strains.** Fold change of average MS1 intensity
1204 and p-value for the GFP-D1 and GFP-Prod strains relative to the NLS-GFP control strain
1205 are shown for detected proteins. Proteins pulled down by GFP-D1 and GFP-Prod
1206 ($log_2FC>1$, $p<0.05$) are highlighted in yellow.

1207

1208 **Supplementary Table 2. List of proteins detected by LC-MS/MS in ovary lysates from**
1209 **GFP-D1, GFP-Prod and NLS-GFP strains.** Fold change of average MS1 intensity and p-
1210 value for the GFP-D1 and GFP-Prod strains relative to the NLS-GFP control strain are
1211 shown for detected proteins. Proteins pulled down by GFP-D1 and GFP-Prod ($log_2FC>1$,
1212 $p<0.05$) are highlighted in yellow.

1213

1214 **Supplementary Table 3. List of proteins detected by LC-MS/MS in GSC-enriched**
1215 **testes lysates from GFP-D1 and NLS-GFP strains.** Fold change of average MS1 intensity
1216 and p-value for the GFP-D1 strain relative to the NLS-GFP control strain are shown for
1217 detected proteins.

1218

1219 **Supplementary Table 4. ipTM scores of D1 and Prod interactors based on AFM**
1220 **structural models.**

1221

1222 **Supplementary Table 5. List of proteins associated with DNA repair in *Drosophila*.**

1223

1224 **Supplementary Table 6. List of proteins associated with transposon repression in**
1225 ***Drosophila*.**

1226

1227 **Supplementary Table 7. List of proteins detected by LC-MS/MS in embryonic lysates**

1228 **from GFP-Piwi and NLS-GFP strains.** Fold change of average MS1 intensity and p-value

1229 for the GFP-Piwi strain relative to the NLS-GFP control strain is shown for detected

1230 proteins.

1231

1232 **Supplementary Table 8. ipTM scores of protein pairs based on AFM structural models.**

1233

1234 **Supplementary Table 9. Differentially expressed genes and TE families between *D1***

1235 **heterozygous and *D1* mutant ovaries in a *chk2*^{6006} background.** Identified genes were

1236 cross-referenced against genes implicated in TE silencing from supplementary table 6.